

OAK RIDGE NATIONAL LABORATORY

operated by

UNION CARBIDE CORPORATION

for the

U.S. ATOMIC ENERGY COMMISSION



ORNL-TM-112-*Scf*
135

UNIT OPERATIONS SECTION MONTHLY PROGRESS REPORT

September 1961

NOTICE

This document contains information of a preliminary nature and was prepared primarily for internal use at the Oak Ridge National Laboratory. It is subject to revision or correction and therefore does not represent a final report. The information is not to be abstracted, reprinted or otherwise given public dissemination without the approval of the ORNL patent branch, Legal and Information Control Department.

LEGAL NOTICE

This report was prepared as an account of Government sponsored work. Neither the United States, nor the Commission, nor any person acting on behalf of the Commission:

- A. Makes any warranty or representation, expressed or implied, with respect to the accuracy, completeness, or usefulness of the information contained in this report, or that the use of any information, apparatus, method, or process disclosed in this report may not infringe privately owned rights; or
- B. Assumes any liabilities with respect to the use of, or for damages resulting from the use of any information, apparatus, method, or process disclosed in this report.

As used in the above, "person acting on behalf of the Commission" includes any employee or contractor of the Commission, or employee of such contractor, to the extent that such employee or contractor of the Commission, or employee of such contractor prepares, disseminates, or provides access to, any information pursuant to his employment or contract with the Commission, or his employment with such contractor.

ORNL-TM-112

UNIT OPERATIONS SECTION MONTHLY PROGRESS REPORT

September 1961

CHEMICAL TECHNOLOGY DIVISION

M. E. Whatley

P. A. Haas

R. W. Horton

A. D. Ryon

J. C. Suddath

C. D. Watson

Date Issued

APR - 5 1962

OAK RIDGE NATIONAL LABORATORY
Oak Ridge, Tennessee
Operated By
UNION CARBIDE CORPORATION
for the
U. S. Atomic Energy Commission

ABSTRACT

Nine samples of $\text{ThO}_2\text{-UO}_2$ prepared as part of the sol-gel process development studies showed no consistent effects from small variations in several process parameters. The reaction of methane and copper oxide was studied. Engineering studies of the continuous dissolution of simulated U-Zr-Sn fuels in 6.5 M NH_4F , 0.6-1.0 M NH_4NO_3 , 0.1 M H_2O_2 were continued in modified 6-in.-dia equipment. A total of 1624 kg of uranium from NaK bonded SRE Core I fuel rods has been dejacketed to date. Initial operability tests of the 250 ton prototype shear unit showed a number of minor modifications are warranted. Center tube temperatures measured in a vertical 64 tube electrically heated simulated fuel element bundle have been very near those previously obtained in the horizontal position. A 304 SS tube containing eutectic NaK was dissolved by HF in fused salt at a tube wall penetration rate of ~2 mils/hr. Partial differential equations were derived from the concentration of unreacted UF_6 as a function of time and position in a sphere of NaF during sorption of UF_6 . Calcium nitrate solution was added directly to the pot calciner during Purex feeding to give smoother operation of the feeding system.

CONTENTS

	<u>Page</u>
Abstract	2
Previous Reports in this Series for the Year 1961	4
Summary	5
1.0 Fuel Cycle Development	7
2.0 GCR Coolant Purification Studies	11
3.0 Power Reactor Fuel Processing	22
4.0 Reactor Evaluation Studies	35
5.0 Volatility	42
6.0 Waste Processing	56

Previous Reports in this Series for the Year 1961

January	ORNL CF 61-1-27
February	ORNL CF 61-2-65
March	ORNL CF 61-3-67
April	ORNL-TM-32
May	ORNL-TM-33
June	ORNL-TM-34
July	ORNL-TM-35
August	ORNL-TM-65

All previous reports in this series are listed in the June 1961 report, ORNL-TM-34, from the beginning, December 1954.

SUMMARY

1.0 FUEL CYCLE DEVELOPMENT

The results of nine samples of ThO₂-UO₂ prepared as part of the sol-gel process development studies showed no consistent effects from the precursor oxide N/Th mole ratio, precursor oxide air firing, sol N/Th ratios of 0.09 to 0.13, sol depth at the start of drying, or small visible porosity or shape differences. Small process variations do not appear critical with respect to obtaining the 8.5 g/cc minimum density required for the BNL ThO₂-U(233)O₂ elements.

2.0 GCR COOLANT PURIFICATION STUDIES

The reaction of methane and copper oxide was studied under conditions expected in Gas Cooled Reactor systems and reaction rate constants were determined. An activation energy of 15 kcal/g-mole CuO reacted was predicted from the variation of the rate constant with temperature in the range 400 to 600°C.

3.0 POWER REACTOR FUEL PROCESSING

3.1 Continuous Modified Zirflex

Engineering studies of the continuous dissolution of simulated U-Zr-Sn fuels in 6.5 M NH₄F, 0.6-1.0 M NH₄NO₃, 0.1 M H₂O₂ were continued in modified 6-in.-dia equipment. Stable performance and satisfactory steady-state operation was achieved. The rates measured were those predicted by experiments in 2-in.-dia equipment with but little increase when the NH₄OH-containing overhead condensate was withdrawn rather than refluxed. Steady-state operation at F/S = 0.08 produced reaction rates ~5.6 mg/cm²-min resulting in loadings ~70 g Zircaloy-2/liter. The loading was raised to ~75 g Zircaloy-2/liter by lowering the feed rate (F/S = 0.06) but the throughput was lowered also (reaction rate = 4.5 mg/cm²-min).

3.2 SRE Dejacketing Studies

Mechanical dejacketing of NaK bonded SRE Core I fuel rods progressed satisfactorily by the dejacketing of ~9-5/7 clusters, producing 668 kg of uranium for aqueous dissolution. A total of 1624 kg of uranium has been dejacketed to date, and only ~200 kg of the SRE fuel remains to be processed. The experimental production rate was ~6.0 kg U/hr, about 3 times this rate would be expected from actual assembly line processing. Analysis from the 100 ml NaK eutectic bond per rod shows a Cs¹³⁷ concentration from 2 x 10⁷ to 2 x 10⁸ dpm/ml.

3.3 Shear and Leach

The economic and technological feasibility of shearing and leaching spent reactor fuels is to be determined initially in a "cold" chop and leach facility consisting of a shear, feeder, leacher, and compactor.

In initial operability tests of the 250 ton prototype shear the unit performed satisfactorily, but a number of minor modifications are warranted to facilitate better operation. Modifications include improving the operation of the feed mechanism and fuel assembly length indicator and re-machining the inner gag to facilitate easier removal from the shear.

4.0 REACTOR EVALUATION STUDIES

Heat Transfer from Spent Reactor Fuels during Shipping

Center tube temperatures measured in a vertical 64 tube bundle have been very near those previously obtained in the horizontal position. A proposed calculational procedure for predicting the temperature distribution gives values in very good agreement with experimental temperatures near the center of the bundle, but near the outside of the bundle the predicted temperatures are too optimistic. The good agreement near the center probably results from an accidental canceling of an optimistic error in calculating the outside tube temperatures and a conservative error in calculating the temperature increases within the bundle.

Convective current effects have been demonstrated by temperature distribution measurements at various positions up the bundle.

5.0 VOLATILITY

A 304 SS tube containing eutectic NaK was dissolved by HF in fused salt at a tube wall penetration rate of ~2 mils/hr. A molten salt splash into the off-gas line occurred during the dissolution run, apparently at the time that the NaK was released from the tube. This was a minor event, since there were only about 3 in. freeboard in the vessel. No change in reactor temperature was noted.

Partial differential equations were derived for the concentration of unreacted UF_6 as a function of time and position in a sphere of NaF during sorption of UF_6 . The model includes the effects of (1) stagnant gas film resistance, (2) rate of diffusion of UF_6 in pores of sphere, (3) reaction rate at the pore walls, and (4) effect of local UF_6 loading on the rate of transport and rate of reaction. The equations were converted to finite difference form in preparation of numerical solution.

6.0 WASTE PROCESSING

Calcium nitrate solution was added directly to the pot calciner during Purex feeding, rather than adding to the feed prior to evaporation, resulting in smoother operation of the feeding system. Sulfate was retained by the solids although the calcium and sulfate were not added to the calciner in stoichiometric balance throughout the test. An interruption of the test at the end of the first hour caused a number of difficulties when the test was restarted.

1.0 FUEL CYCLE DEVELOPMENT

P. A. Haas

Preparation of high density $\text{ThO}_2\text{-UO}_2$ particles and vibratory compaction into cladding tubes will be pursued by development of fuel elements containing U-233 for BNL. The present emphasis is on process development necessary for the conceptual design of this pilot plant. The Unit Operations studies include denitration, sol dispersion, sol drying, and calcination procedures. Oxide products on a kg scale are being supplied for vibratory compaction development.

1.1 Sol-Gel Process Development - C. C. Haws, Jr., J. W. Snider, R. D. Arthur

A series of mixed oxide samples was prepared from trough denitrator products representing the following variations in feed materials:

1. A low N/Th ratio standard product (Table 1.1, run 27).
2. A high N/Th ratio product, standard except for an overnight air firing at 700°C (run 16).
3. A low N/Th ratio standard product except for an overnight firing at 700°C (run 35-1).
4. A low N/Th ratio standard product except that the usual denitration step was followed by a 3-hr air firing at 425°C. This post denitration air firing was done in the trough denitrator.

The sols obtained from two of the above materials were also dried from different depths to determine the effect of depth upon shard properties and production rate.

The samples prepared from the 700°C air-fired feed material did not reach any higher particle density nor any higher vibrated density than did the other materials. The two samples taken from these batches, however, did show excellent reproducibility of results. These results show that the 700°C firing step is not required to obtain a satisfactory compacted density.

After the 1150°C sintering step all samples of this series were examined visually for porosity and shape. The two samples selected as the best in appearance were run 27, 1 in.; and run 40, 3/4 in. The other samples had varying degrees of porosity, but were not significantly inferior in shape. The only sample not meeting the 8.5 g/cc minimum vibratory density requirement was the apparently excellent run 27, 1 in. The vibratory compaction results on this series show that appearance is of questionable usefulness as a means of predicting the compactibility of a preparation.

The sampling-analytical error is apparently large enough to obscure any relationship between particle (toluene) density and any other shard property (Table 1.1).

Table 1.1. Properties of Mixed Oxides (ThO₂-UO₂) Prepared by Sol-Gel Process

- Conditions: 1. Thoria precursor prepared in agitated trough denitrator
 2. Uranium added as ammonium diuranate
 3. Shards sintered at 1150°C before H₂ reduction

Run No.	Initial N/Th Ratio	Dispersed N/Th Ratio	Wt % U	Sol Drying Depth, in.	Particle Density, ^a g/cc		Vibrated Density, g/cc	
					Before H ₂ Reduction	After H ₂ Reduction	5/16-in.-dia Tube	1/2-in.-dia Tube
16	0.11	0.09	3	2	10.0	9.83 9.97	8.72 8.74	
27	0.09	0.13	3	1	9.80	9.82 9.75	8.38 8.38	8.58
			3	1-1/2	9.77	9.92	8.62	-
			3	2	9.66	9.94	8.72 8.74	
35-1	0.07	0.09	3	2	9.97	9.82 9.99	8.70 8.73	
40	0.035	0.13	4	3/4	9.74	9.86 9.86	8.64 8.63	
			4	1	9.81	9.81	8.76	
			4	2	9.80	9.90	8.70 8.50	8.54
40C ^b			4	-	-	-	-	8.50

^aDetermined pycnometrically with toluene.

^bThis composite sample was prepared from equal weights taken from each of the three preceding run 40 batches.

The 1/2-in. tube is the fuel rod diameter intended for future applications of Sol-Gel materials and the tube has consistently given higher densities than the 5/16-in.-dia test in the past. The vibratory compactions above are anomalous, i.e. the density of one product increased (run 27, 1 in.) while the other run (run 40 composite) decreased when going from 5/16-in. to 1/2-in. tubes. Both these tests gave results ≥ 8.5 g/cc which is the minimum acceptable density.

Within the range of the study there was no significant effect arising from either the initial N/Th ratio of a precursor material or the N/Th ratio at which a preparation is dispersed. The 0.13 N/Th dispersal ratio has been accepted as an optimum and yet the 0.09 material appears equal to the 0.13 material in all respects. Similarly the properties of the samples prepared from low N/Th ratio precursor materials, i.e. 0.035, are the equal of those prepared from the higher, i.e. 0.09, precursors.

The sol depth at the beginning of the evaporation-drying step has no effect upon the yield of shards for the mixed oxides. This is contrary to experience with pure thoria sols. The throughput for the evaporating oven for an initial 1 in. sol depth was 60 g/hr-ft² of evaporating-drying surface (Table 1.2).

Plunge heating of the 500°C pre-fired material to ~1200°C has been practiced. In order to heat the pre-fired material as quickly as possible the size and bed depth of the sample to be plunged have been limited. In a single test on this process variation, run 35-1 product consisting of 937 g was plunge heated in a 2-in. deep bed. Prior samples have weighed ~200 g and were fired in 1-in. beds. No ill effects were apparent in this single test. Further testing of this variation will be made.

The tentative conclusion reached is that the present Sol-Gel procedure will provide material compacting to the minimum required density (8.5 g/cc) in a 1/2-in. tube and that the variables examined above have little significant effect upon product quality over a reasonable range.

Table 1.2. The Effect of Initial Sol Depth upon Shard

Size and Sol Drying Rate

Conditions: 1. Oven at 80°C
2. 2.0 M thoria-urania in original sol

Run No.	Original Sol Depth (in.)	Percent of Shards > 16 Mesh	g Solids Produced per hr per ft ² Drying Surface
27	1	92	60
	1-1/2	94	102
	2	94	76
40	3/4	93	-
	1	94	-
	2	94	-

2.0 GCR COOLANT PURIFICATION STUDIES

J. C. Suddath

2.1 Differential Bed Tests on CH₄-CuO Reaction - C. D. Scott

A series of tests were made in which flowing streams of He containing less than 5% CH₄ were sent through differential beds of CuO pellets. These tests were made in the temperature range of 400-600°C and at two pressures, 1 atm and 20.4 atm. The tests made at 1 atm used a thermal balance (Figure 2.1) in which the weight change of the bed was periodically recorded and the tests made at 20.4 atm were in a closed reactor with initial and final bed weights taken. Operating conditions for these tests are listed in Table 2.1.

The thermal balance runs were made by introducing 5.0 slpm of pre-heated He at 1 atm containing CH₄ into the heated reaction tube which contained the differential bed in a platinum basket. The platinum basket was connected to a balance whose accuracy was ± 0.01 g. Bed weights were determined every 10 min and the CH₄ concentration in the entering and effluent gas was determined by a gas adsorption chromatograph.

The high-pressure tests were made in the oxidizing vessels of the Helium Coolant Purification Test Facility (Unit Operations Monthly Progress Report, May 1961). In these tests, the preheated helium, contaminated with CH₄, was introduced to the 2-in.-dia reaction vessel where it passed through a differential bed of CuO pellets with a sufficient velocity to prevent external mass transfer resistance. Each run lasted a specific length of time (Table 2.1) and the CH₄ concentration of the effluent stream was measured periodically by a gas adsorption chromatograph.

2.2 Kinetics of the CH₄-CuO Reaction

Unlike the mass transfer dependence of the reactions of H₂ or CO with CuO, the CH₄-CuO reaction appears to be dependent on the availability of actual CuO surface area. Microscopic examination of the copper oxide pellets after partial reduction by CH₄ showed that there was no Cu-CuO interface in the pellet as a whole but rather in the individual CuO particles which made up the pellet. This indicates that mass transport of CH₄ to and through the pellet is not a factor. Since mass transport through the small CuO particles was not a factor in the CO-CuO reaction, it is assumed that in the CH₄-CuO reaction, a much slower reaction, the transport of the CH₄ through the small CuO particle was also not a factor. There were individual Cu-CuO interfaces in each small CuO particle, therefore, it will be assumed that the CH₄-CuO reaction is dependent on the amount of Cu-CuO interface or on the amount of actual CuO surface available for reaction. It will also be assumed that the reaction rate is dependent on the CH₄ concentration in the gas phase.

On this basis, the reaction rate of CH₄ with CuO may be expressed as

UNCLASSIFIED
ORNL-LR-DWG 65307

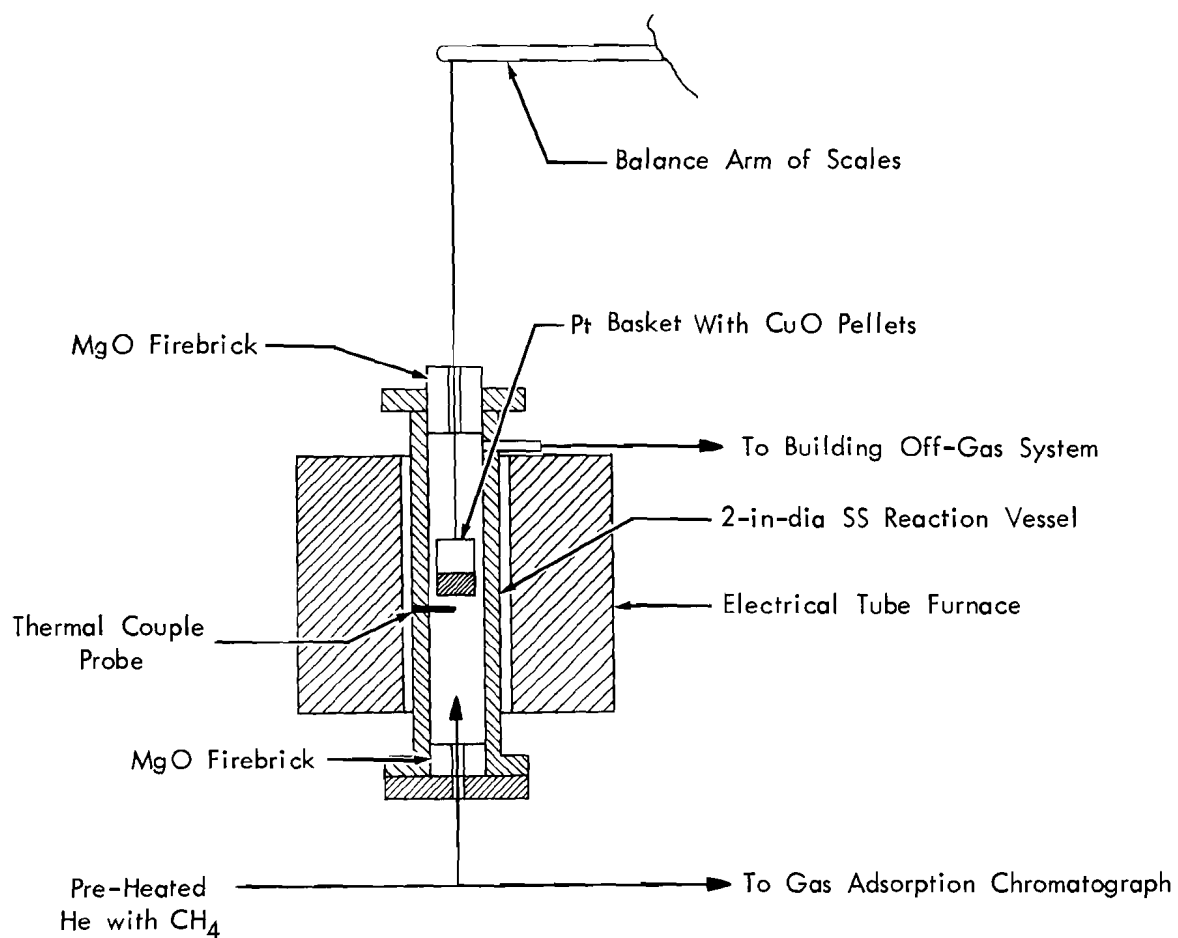


Fig. 2.1. Thermal balance set-up used in differential bed tests of the CH_4 - CuO reaction.

Table 2.1. Experimental Conditions of CH₄-CuO

Differential Bed Tests

Run No.	Type of Test	Temperature, °C	CH ₄ Concentration, g-moles/cc	Pressure, atm
TB-1	Thermal balance	500	2.1×10^{-7}	1.0
TB-2	Thermal balance	600	6.5×10^{-7}	1.0
TB-3	Thermal balance	400	2.5×10^{-7}	1.0
TB-4	Thermal balance	500	1.37×10^{-7}	1.0
DR-1	Closed vessel	400	4.26×10^{-6}	20.4
DR-2	Closed vessel	500	2.02×10^{-6}	20.4
DR-3	Closed vessel	500	5.05×10^{-6}	20.4
DR-4	Closed vessel	500	1.64×10^{-6}	20.4
DR-5	Closed vessel	600	2.42×10^{-6}	20.4

$$\frac{dn}{dt} = -kCS \quad (1)$$

where

n = molar volume of unreacted CuO, g-moles/cc bed

t = run time, sec

C = CH₄ concentration, g-moles/cc

S = specific surface area based on average size of CuO particle in pellet, cm²/cc bed

k = reaction rate constant, cm/sec

The specific surface area, S , may be shown to be

$$S = (4\pi E)^{1/3} \left(\frac{3n}{d}\right)^{2/3} \quad (2)$$

where

E = small CuO particle density, particles/cc bed

d = density of small CuO particles, g-moles/cc bed

Let

$$K = (4\pi E)^{1/3} (3/d)^{2/3} \quad (3)$$

then eq. (1) becomes

$$\frac{dn}{dt} = -kKn^{2/3} \quad (4)$$

Equation (4) can be integrated and the resulting expression can be solved for the reaction rate constant, k ,

$$k = \frac{n_o^{1/3} - n^{1/3}}{Kt} \quad (5)$$

Equation (5) is valid if the CH₄ concentration, C , is constant.

Equation (5) can be used to determine the reaction rate constant, k , for each of the differential bed tests. In the case of the thermal balance tests, several experimental points can be used to determine k for each test while for the high pressure tests only one point will be available.

It was found that the reaction rate constant, k , was not a function of CH_4 concentration or pressure, however, it did vary with temperature (Table 2.2). An Arrhenius type expression can be used to express k in the temperature range of 400-600°C (Figure 2.2)

$$k = 51e^{-7590/T} \quad (6)$$

This represents an activation energy of ~15 kcal/g-mole CuO reacted.

Equation (5) can be rearranged to give the CuO molar volume, n

$$n = (n_o^{1/3} - kKct)^3 \quad (7)$$

Equation (7) with the values of k predicted from eq. (6) can then be used to compare experimental weight losses in the thermal balance runs with the predicted weight losses based on the assumed reaction rate dependence. It was found that there was fair agreement in the two values (Figures 2.3-2.6). Thus, it is assumed that the reaction rate dependence can be expressed by eq. (1) and this expression will be used to predict effluent CH_4 concentrations in deep bed tests.

Table 2.2. Reaction Rate Constant as Determined
from Differential Bed Tests

Run No.	Run Time, sec	Temp., °C	k, cm/sec
TB-1	3000	500	0.00304
	6000	500	0.00321
	9000	500	0.00291
	12000	500	0.00241
	Average		0.00290
TB-2	3000	600	0.00730
	6000	600	0.00806
	9000	600	0.00880
	12000	600	0.00885
	15000	600	0.00840
	18000	600	0.00846
	Average		0.00831
TB-3	3000	400	0.00055
	6000	400	0.00045
	Average		0.00050
TB-4	3000	500	0.00239
	6000	500	0.00210
	9000	500	0.00237
	12000	500	0.00231
	15000	500	0.00248
	18000	500	0.00265
	Average		0.00238
DR-1	1800	400	0.00076
DR-2	1800	500	0.00231
DR-3	3600	500	0.00352
DR-4	3600	500	0.00333
DR-5	1800	600	0.00728

UNCLASSIFIED
ORNL-LR-DWG 65308

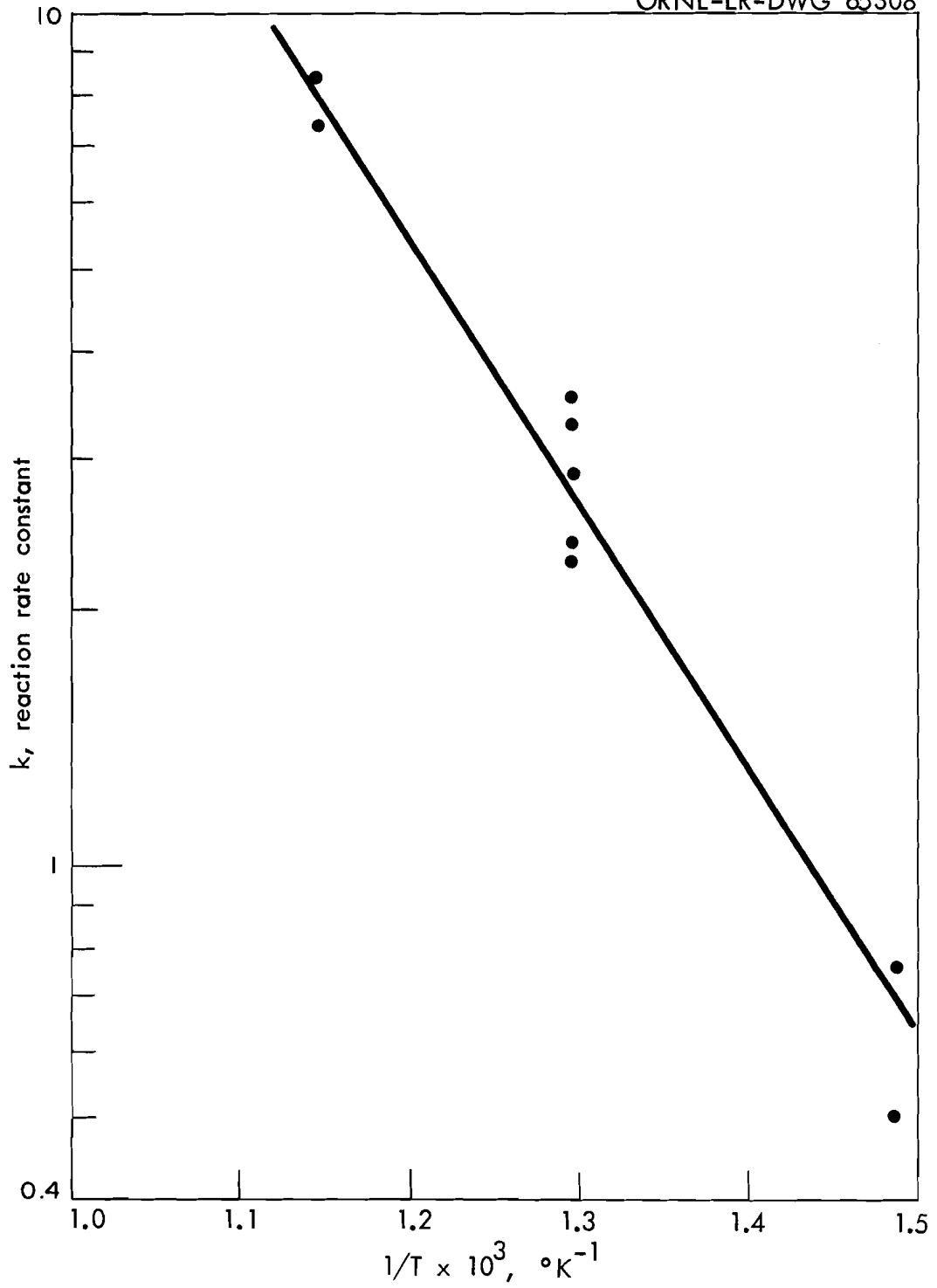


Fig. 2.2. Arrhenius plot of reaction rate constant for the reaction of CH_4 in a flowing stream of helium with a fixed bed of CuO as determined from differential bed tests. The reaction rate was assumed to be proportional to CH_4 concentration and CuO surface area.

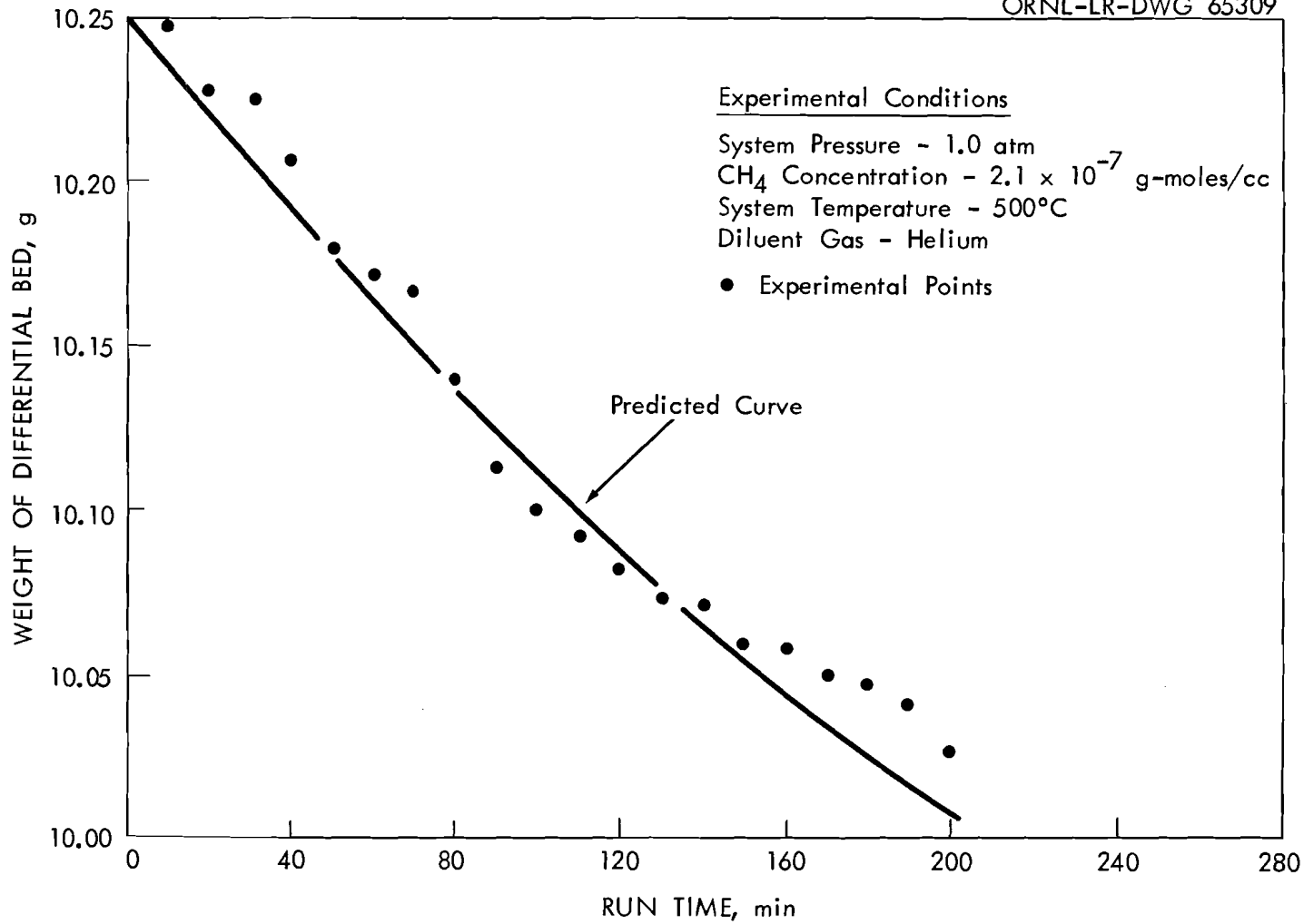


Fig. 2.3. Comparison between experimental results for thermal balance Run TB-1 and results predicted from the reaction rate being proportional to CH₄ concentration and CuO surface area.

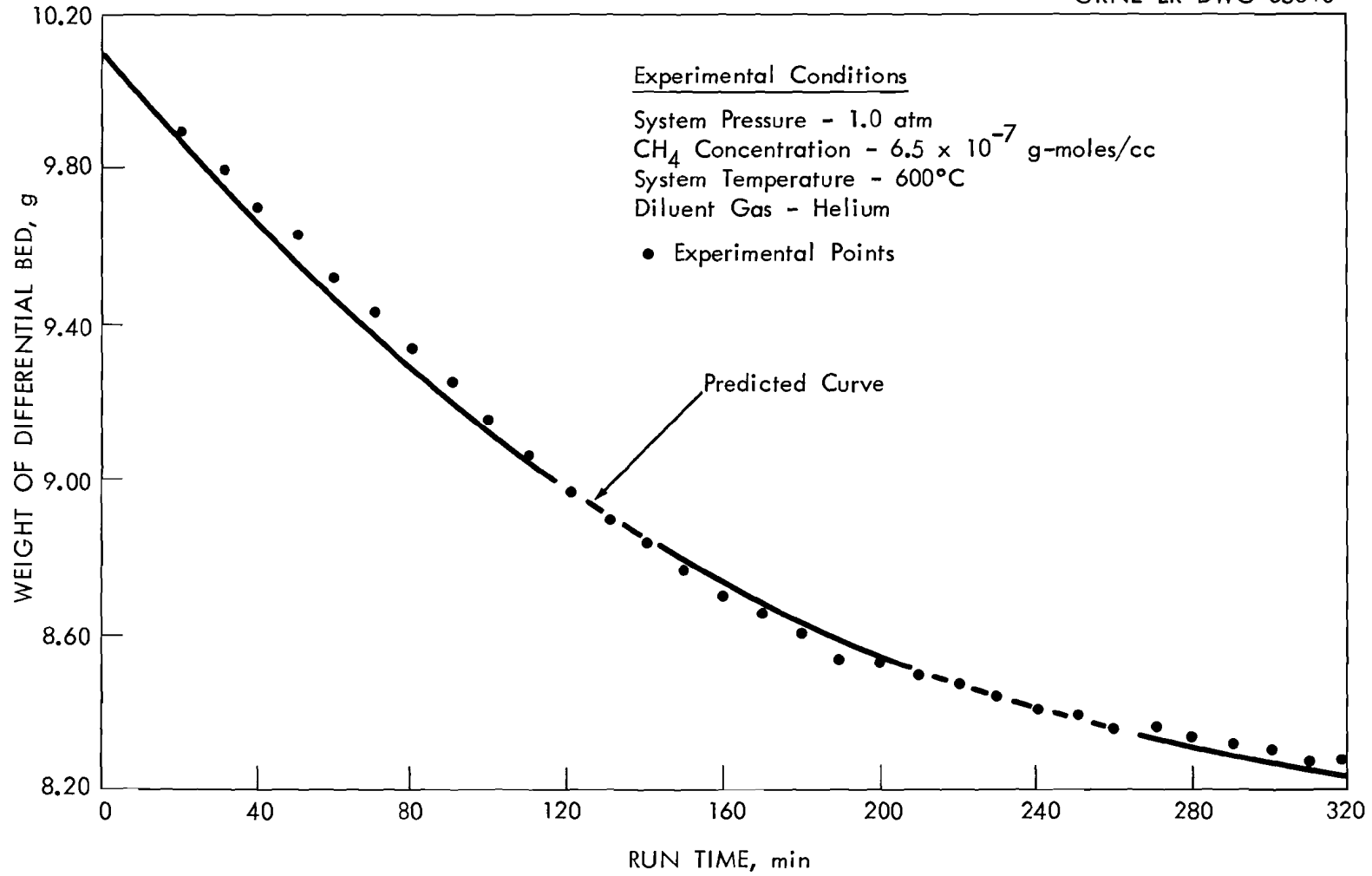


Fig. 2.4. Comparison between experimental results for thermal balance Run TB-2 and results predicted from the reaction rate being proportional to CH₄ concentration and CuO surface area.

UNCLASSIFIED
ORNL-LR-DWG 65311

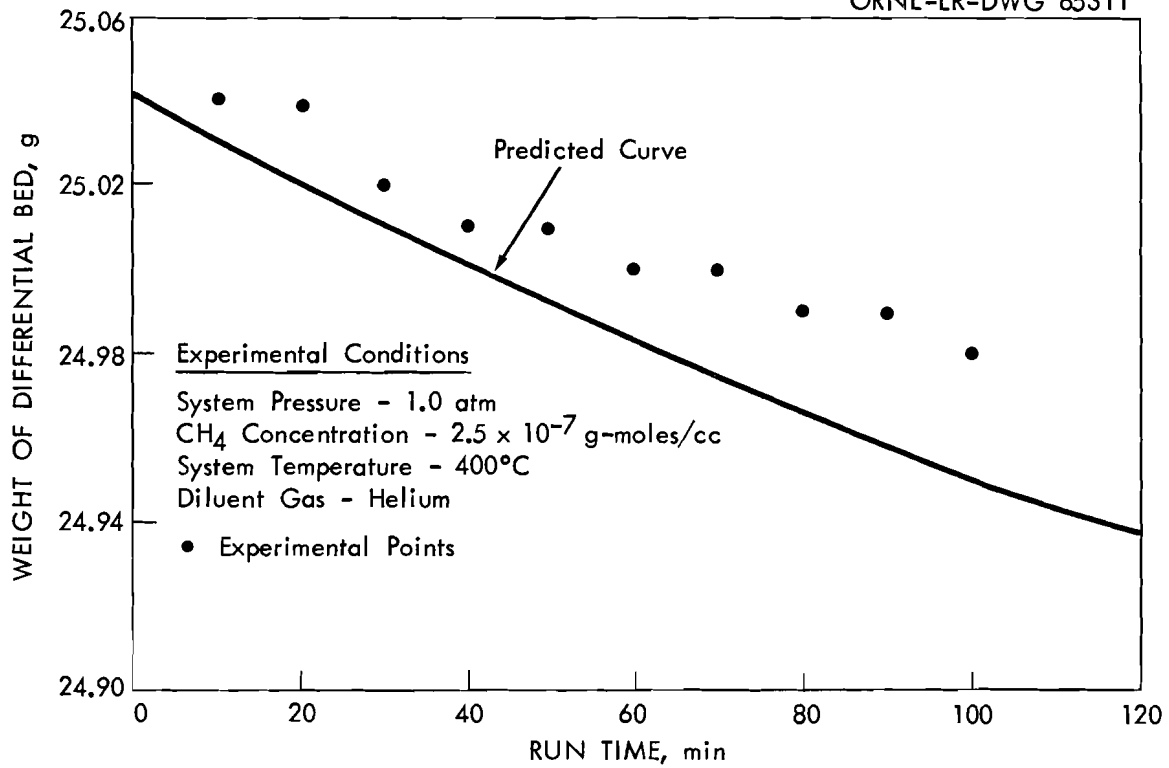


Fig. 2.5. Comparison between experimental results for thermal balance Run TB-3 and results predicted from the reaction rate being proportional to CH₄ concentration and CuO surface area.

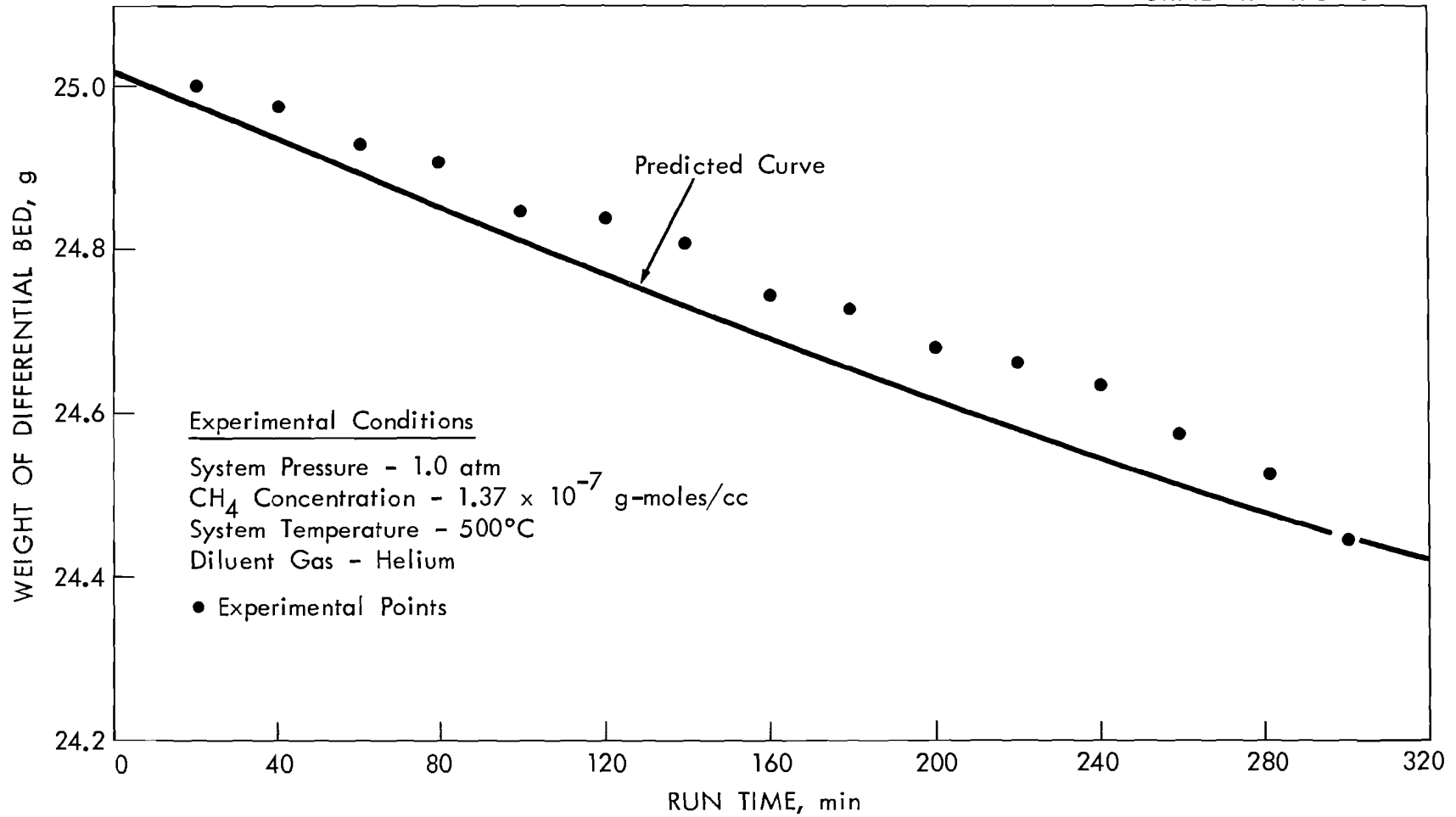


Fig. 2.6. Comparison between experimental results for thermal balance Run TB-4 and results predicted from the reaction rate being proportional to CH₄ concentration and CuO surface area.

3.0 POWER REACTOR FUEL PROCESSING

C. D. Watson

3.1 Continuous Modified Zirflex - F. G. Kitts, F. L. Rogers

Modified Zirflex is a process for the recovery of uranium from U-Zr-Sn fuels involving dissolution in $\text{NH}_4\text{F-NH}_4\text{NO}_3\text{-H}_2\text{O}_2$ solutions, stabilization with $\text{HNO}_3\text{-Al}(\text{NO}_3)_3$. Hydrogen peroxide is added to the dissolvent to oxidize U^{IV} to the more soluble U^{VI} so that fuels containing higher percentages of U (up to 10%) can be processed without the intermediate precipitation of UF_4 which would occur if this oxidant were not added. Presently, the relationship between reaction rate and dissolvent feed rate to specimen surface area ratio is being investigated by dissolving Zircaloy-2 in a 6-in.-dia dissolver.

The reaction rate increased as F/S increased but the increase was not linear so that although the amount dissolved (total throughput) increased with increasing F/S, the loading decreased leaving a rather narrow range of operation giving practical dissolution rates and loadings high enough to avoid excessive waste volumes. A reasonable approximation of steady-state operation was shown in all three runs. Apparently a small beneficial effect was observed when the NH_4OH -containing overhead condensate was withdrawn and an equal volume of water was returned to the dissolver.

The complete data for two runs in engineering-scale equipment and the analytical data from a previous run (Unit Operations Monthly Report, August 1961) are reported in Table 3.1 and Figures 3.1 and 3.2. The reaction rate (R), feed rate (F), and specimen surface area (S) are shown in Table 3.1 along with various solution compositions. These three are correlated in Figure 3.1 as reaction rate vs F/S. Figure 3.2 shows the instantaneous zirconium concentration in the dissolver at 5 min intervals over the period of steady-state operation for the three runs. The curved line in Figure 3.1 is the relationship between reaction rate and F/S established by previous work in 2-in.-dia equipment with total reflux of NH_4OH -containing overheads. This shows reaction rate increasing with F/S but at an ever decreasing rate. This means that although total throughput increases, solution loading [$L = R/(F/S)$] decreases with attendant increase in chemical costs and waste volumes. The straight lines are lines of constant zirconium loading and free F^- concentration. The three runs in the 6-in.-dia equipment (indicated on Figure 3.1) probably fit the curve within experimental error; however, some differences should be pointed out. Run 1 was made at total reflux (with rectification) while in runs 2 and 3 the overhead condensate was withdrawn and an equal volume of water was returned. Runs 2 and 3 indicate that higher rates and loadings might be obtained operating at a higher F/S with condensate withdrawal. Run 2 was an exceptional run in that it gave a higher reaction rate than run 1 (made at higher F/S) and a higher loading than run 3 (made at lower F/S). The superiority of run 2 is probably explained by the hump in the curve of dissolver solution Zr M vs time, Figure 3.2. Runs 1 and 3 show relatively steady-state operation while run 2 which should have produced a horizontal line between runs 1 and 3 is displaced upward and more erratic.

Table 3.1. Continuous Modified Zirflex Runs in 6-in.-dia Equipment

Conditions: Boiling, batch dissolution of Zircaloy-2 to provide initial dissolver charge

Run No.	Feed Rate cm ³ /min	Dissolvent			Specimen Area cm ²	Diss Time min	Δ Wt g	Reaction Rate Zircaloy-2 mg/cm ² -min	F/S cm/min	Dissolver Product ^a		Stabilizer			Solvent Extraction Feed ^b			Balance Material	
		NH ₄ F M	NH ₄ NO ₃ M	H ₂ O ₂ M						Dissolver Loading g Zly-2/ℓ	Free F ⁻ M	Vol ℓ	HNO ₃ M	Al(NO ₃) ₃ M	Vol ℓ	Zr M	Total F M	Zr %	F %
1 ^d	330	6.6	0.61	0.1	4046	55	1245	5.60	0.0816	68.63	2.1	15.0	1.8	1.8	30.4	0.36	3.3	90	101
2 ^e	307	6.7	1.0	0.1	4160	50	1191	5.73	0.0738	77.64	1.6	12.8	1.8	1.8	25.5	0.44	-	83 ^c	-
3 ^e	288	6.6	1.0	0.1	4700	60	1271	4.5	0.0613	73.4	1.9	14.0	1.8	1.8	29.5	0.42	3.5	92	90

^a Average values calculated from $L = \frac{R}{F/S}$. See Figure 3.1 for instantaneous experimental values.

^b Also contained ~1 M HNO₃ and ~1 M Al(NO₃)₃.

^c A portion of the dissolution product was lost before stabilization.

^d Total reflux (with rectification).

^e Overhead condensate withdrawn, equal volume of H₂O added.

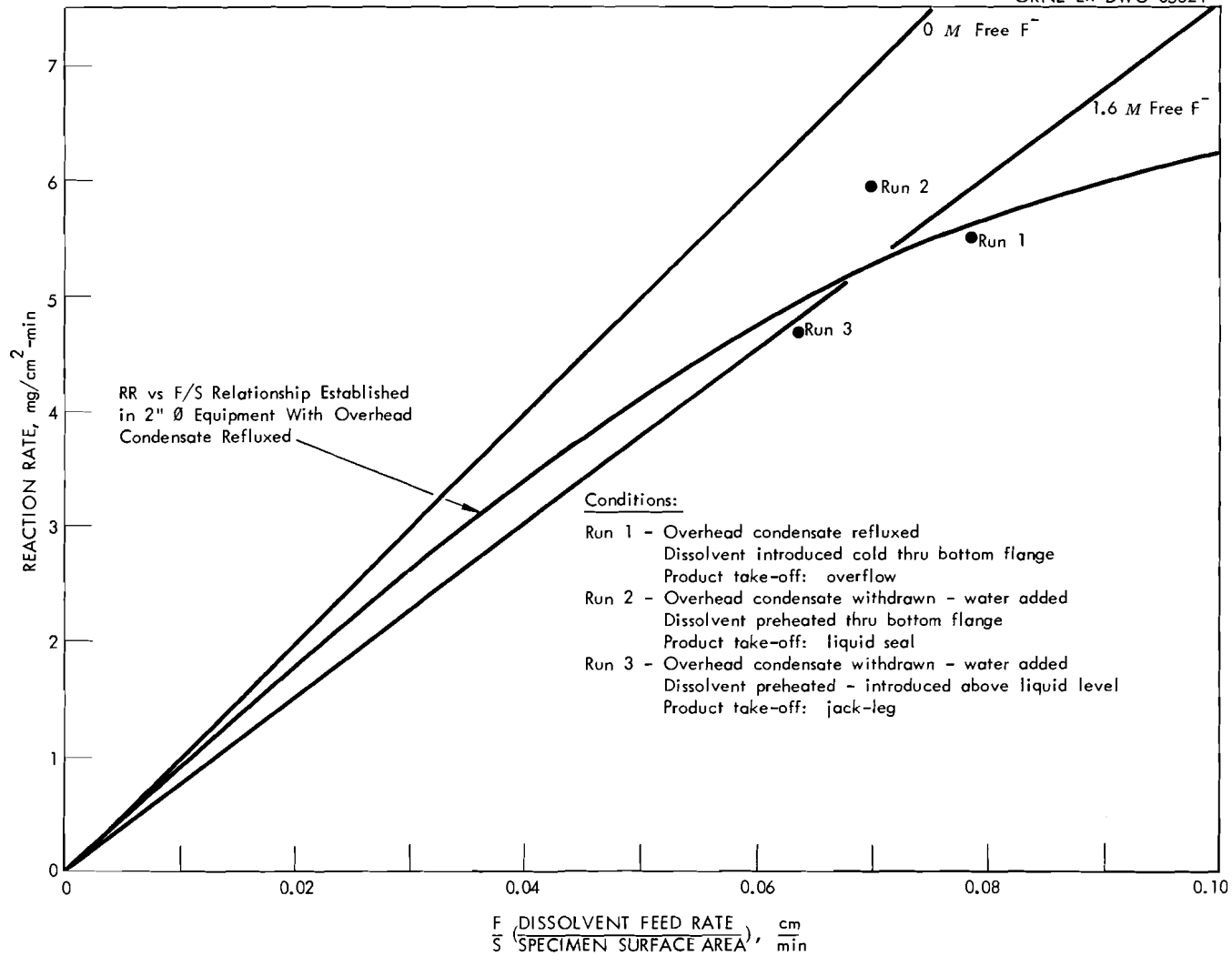


Fig. 3.1. Continuous modified zirflex: correlation of reaction rate dissolvent feed rate and specimen surface area.

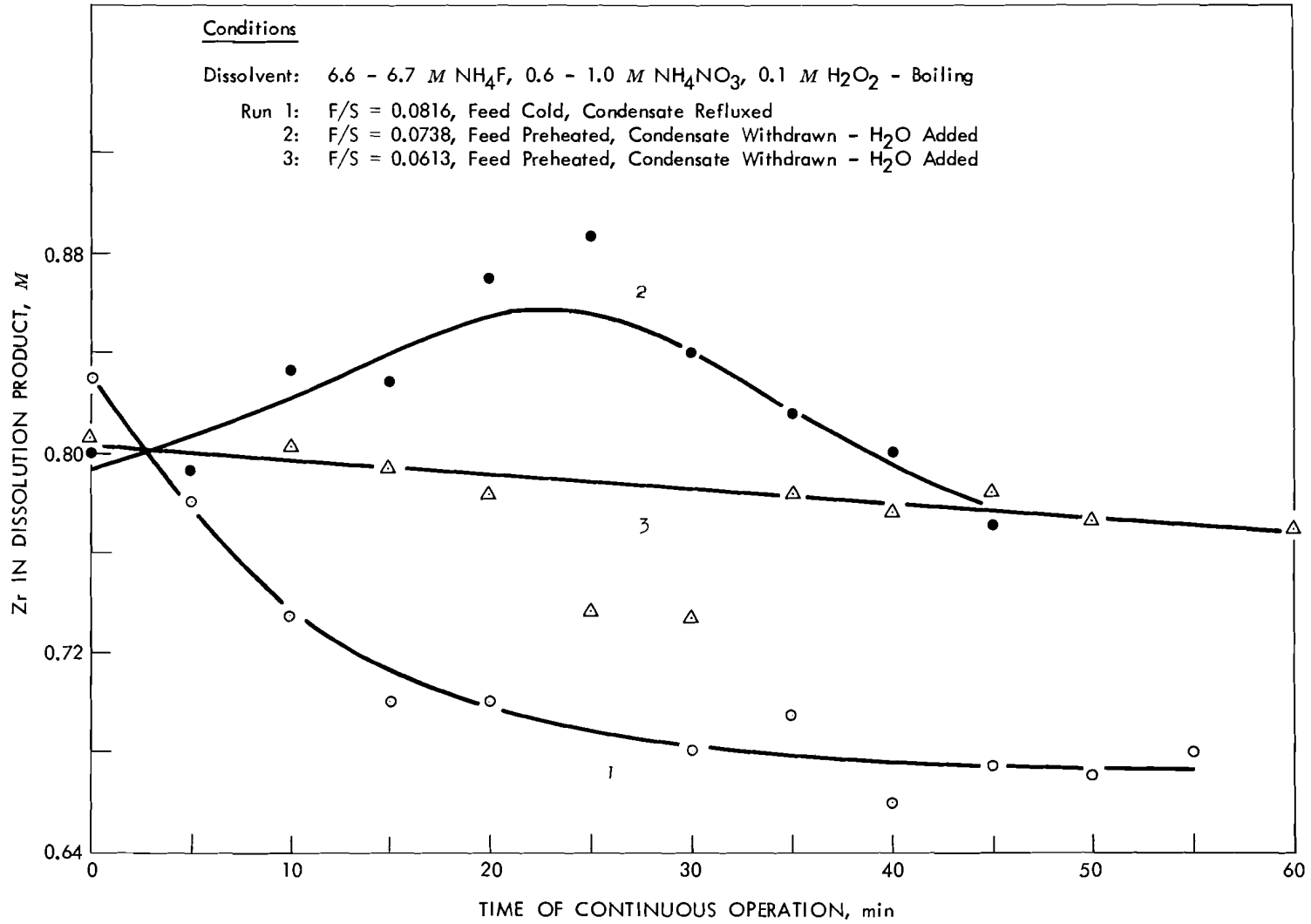


Fig. 3.2. Continuous modified zirflex: steady state Zr concentration in dissolver solution.

All three runs were made by first producing by batch dissolution a dissolver charge of the volume and composition estimated as the steady-state condition. These compositions are shown as time zero in Figure 3.2 and were relatively accurate except in run 1 where a steady reduction in Zr M characterized the approach to steady state. This should result in a low observed dissolution rate since for the first portion of the run dissolution was occurring in a free F^- concentration less than that calculated for the steady-state condition. After the batch dissolution was completed the element was charged (totally immersed) and feed was begun; the dissolver effluent flowed into a batch of stabilizer (Table 3.1) whose volume was 0.8 of the volume expected to overflow from the dissolver. The elements (multiplate, Zircaloy-2, ~ 0.060 -in. thick) were attacked ~ 0.015 -in. so that the error introduced by assuming constant area throughout a run should be less than that caused by changing surface roughness.

The equipment for the three runs differed significantly only in the method of product withdrawal. In run 1 a simple overflow was used with cold dissolvent fed at the bottom; the simple overflow technique with the absence of a liquid seal allowed NH_3 to contact the stabilized product and a flocculent white precipitate was formed. In run 2 a jackleg entering the dissolver adjacent to the reaction zone was used as the overflow device providing a liquid seal, with preheated dissolvent entering the bottom, but operation was hydraulically unstable due to intermittent blowing of the shallow seal. In run 3 satisfactory operation was achieved using a jackleg entering the sidewall of the dissolver near the bottom flange, and feeding preheated dissolvent above the liquid level. The feeding of dissolvent from above should provide for some attack of the ZrO_2 coated elements stacked in the dissolver before they are immersed in the dissolvent.

3.2 SRE De jacketing Studies - G. A. West

Mechanical de jacketing techniques are being demonstrated in the ORNL High Level Segmenting Facility, Bldg. 3026-D, by processing NaK bonded, stainless steel clad uranium fuel from the Sodium Reactor Experiment (SRE), Core I, burned to ~ 675 mwd/ton and decayed ~ 2 years.

Approximately 1630 kg, 91%, of the 1786 kg of uranium delivered to ORNL has been de jacketed, canned and stored for future aqueous dissolution and recovery. The experimental production rate for the past month was ~ 6.0 kg U/hr attained during the de jacketing of 668 kg of uranium. Down time was $\sim 14\%$ of the total operating hours and included time for photographs, movie shots and equipment repair which included changing torn manipulator gauntlets and boots, replacing a decladder cutting wheel, renewing a teflon liner in a valve and O-rings on both the jackscrew and expanding unit of the pusher cylinder. A production plant processing rate would be expected to exceed the experimental rate by a factor of 2 to 3. A total of 6.5 liters of the liquid metal NaK eutectic discharged from the fuel rods was collected and destroyed in batches of ~ 100 ml by reacting it with steam. Analysis of the NaK shows a Cs^{137} concentration of 1×10^6 to 6×10^7 cpm/ml with no detectable plutonium or uranium; gross β of 5×10^6 to 3×10^7 cpm/g and gross γ at 6×10^6 to 2×10^8 cpm/g.

Radiation measurements made on a can of 12 slugs from a single fuel rod and a can of inert stainless steel scrap material from a cluster (about 4.5 kg) was 480 and 120 r/hr, gamma, respectively at contact. Radiation measurements were as follows:

Distance	Slugs (9.9 kg U)		Scrap	
	γ	β, γ	γ	β, γ
Contact (r/hr)	480	5,160	120	1,380
0.5 ft (r/hr)	150	660	37	156
1.0 ft (r/hr)	66	270	21	87
2.0 ft (r/hr)	18	90	7	30

3.3 Shear and Leach - B. C. Finney

A shear and leach program to determine the economic and technological feasibility of continuously leaching the core material (UO_2 or UO_2-ThO_2) from relatively short sections (1-in. long) of fuel elements produced by shearing is continuing. This processing method has the apparent advantage of recovering fissile and fertile material from spent power reactor fuel elements without dissolution of the inert jacketing material and end adapters. These unfueled portions are stored directly in a minimum volume form as solid waste. A "cold" chop leach complex consisting of a shear, conveyor-feeder, and leacher is being evaluated prior to "hot" runs.

The shakedown operations of the 250 ton prototype shear are continuing. A number of minor modifications are being made to facilitate better operation of the shear. These changes include such items as improving the operation of the fuel assembly length indicator, installation of a second hydraulic cylinder at the front of the feed mechanism to provide a smooth motion, and enlarging the arm slot in the inner gag for easier removal.

The relative position of the primary pieces of equipment indicating flow of materials in the shear and leach complex is presented in Figure 3.3. The 250 ton prototype shear consists primarily of a remotely operable shear powered by a hydraulic (oil) system and a hydraulic (water or air) operated feed mechanism (Figure 3.4). The sequence of operating the shear follows: a fuel assembly is picked up with a crane and inserted into the fuel element envelope by means of the loading arm. The pusher arm is moved into position where it pushes the fuel assembly into the shear against a stop initially and after each cut is made (Figure 3.5). A step shaped movable blade shears the fuel assembly into short sections of 1/4-in. to 1-in. Both the stop and step blade are mounted on the ram (Figures 3.6 and 3.7). The fuel assembly is held during shearing by an inner and outer gag and by the fixed blade. After the ram has made a complete stroke (forward and backward) the gags are released so that the fuel assembly can be moved forward against the stop for the next cut.

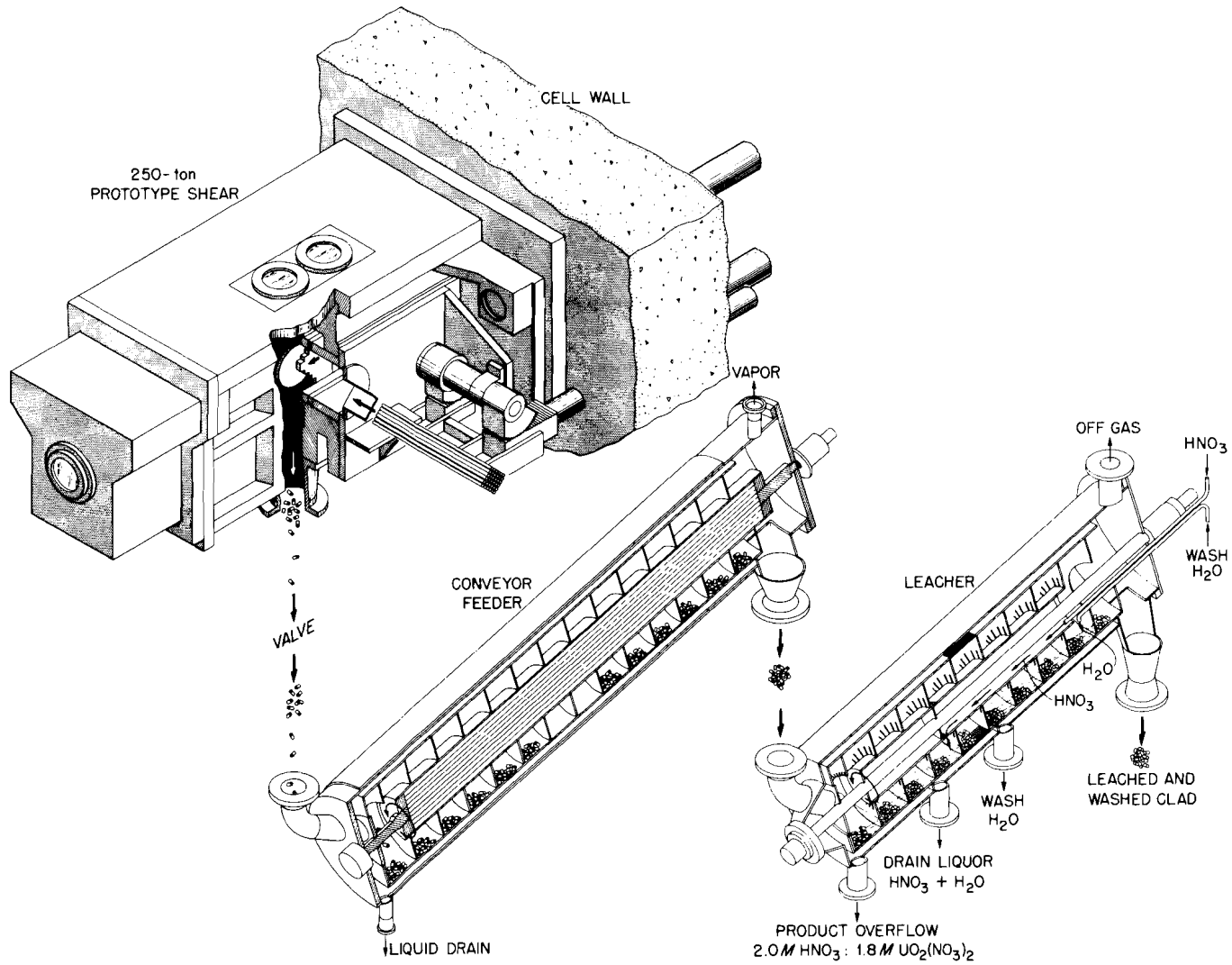


Fig. 3.3. Shear and leach complex indicating relation position of major equipment components and flow of materials.

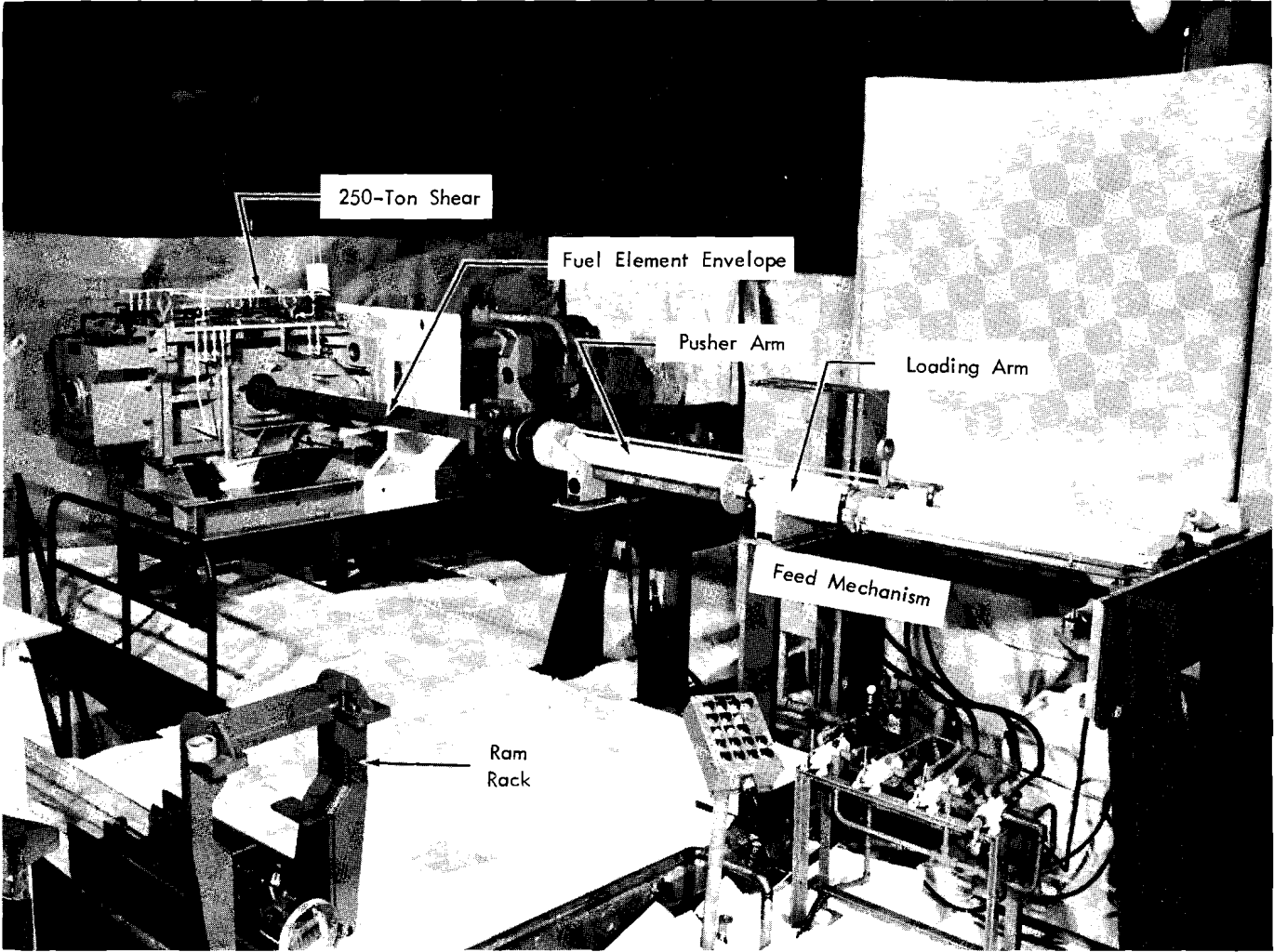


Fig. 3.4. 250-Ton prototype shear and feed mechanism.

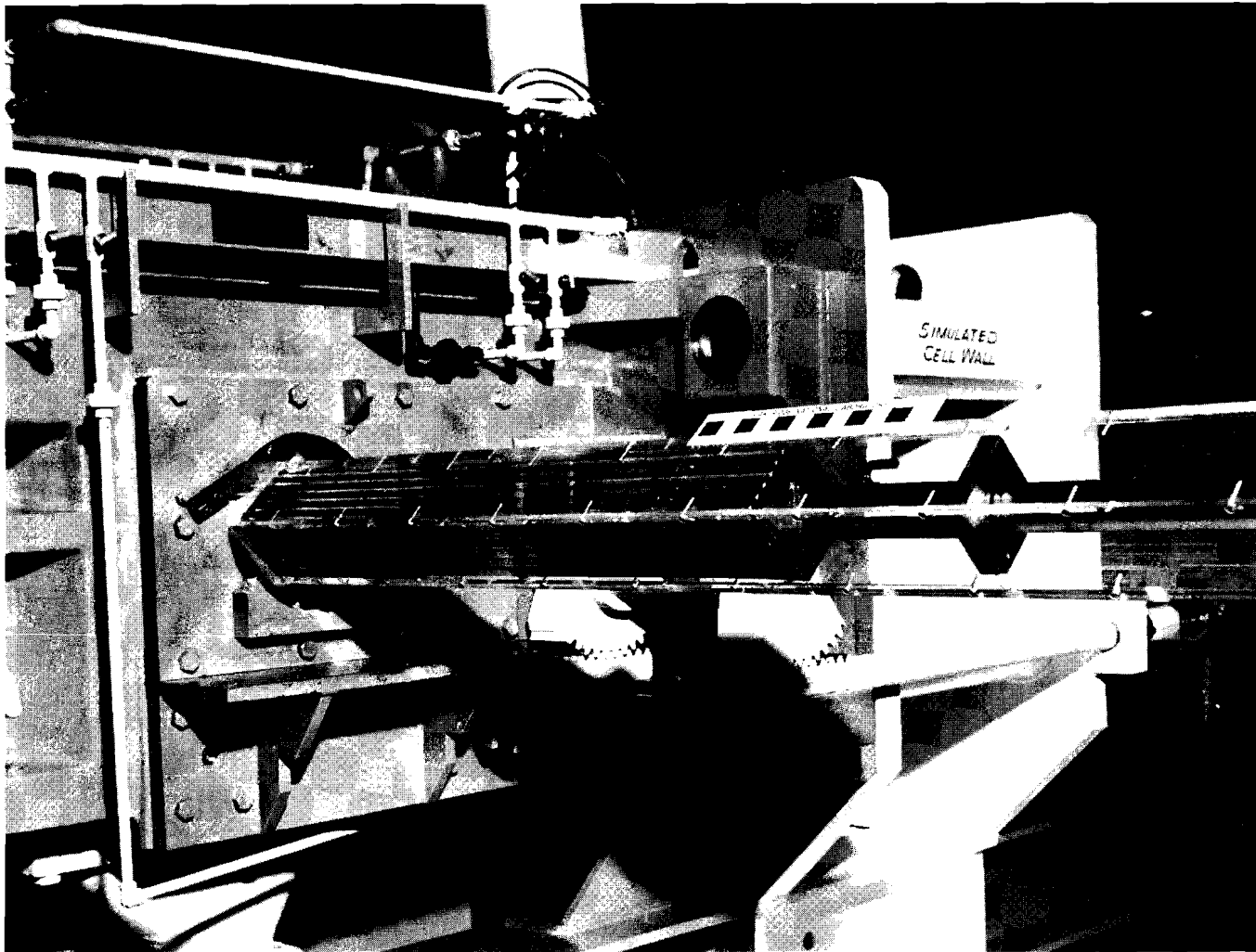


Fig. 3.5. Pusher arm positioning fuel assembly against stop.

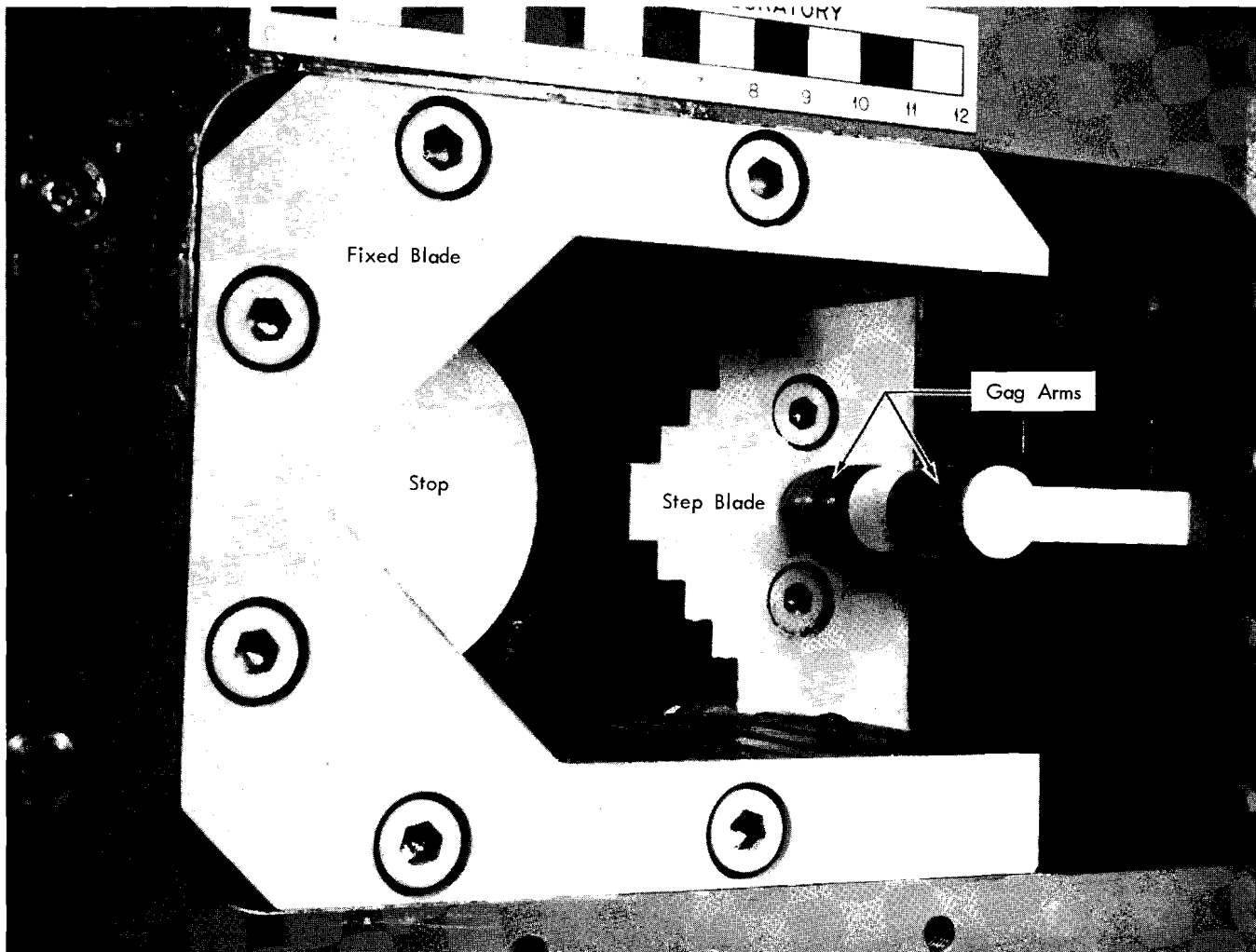


Fig. 3.6. View of step blade, stop, gag arms, and fixed blade with gags and face plate removed.

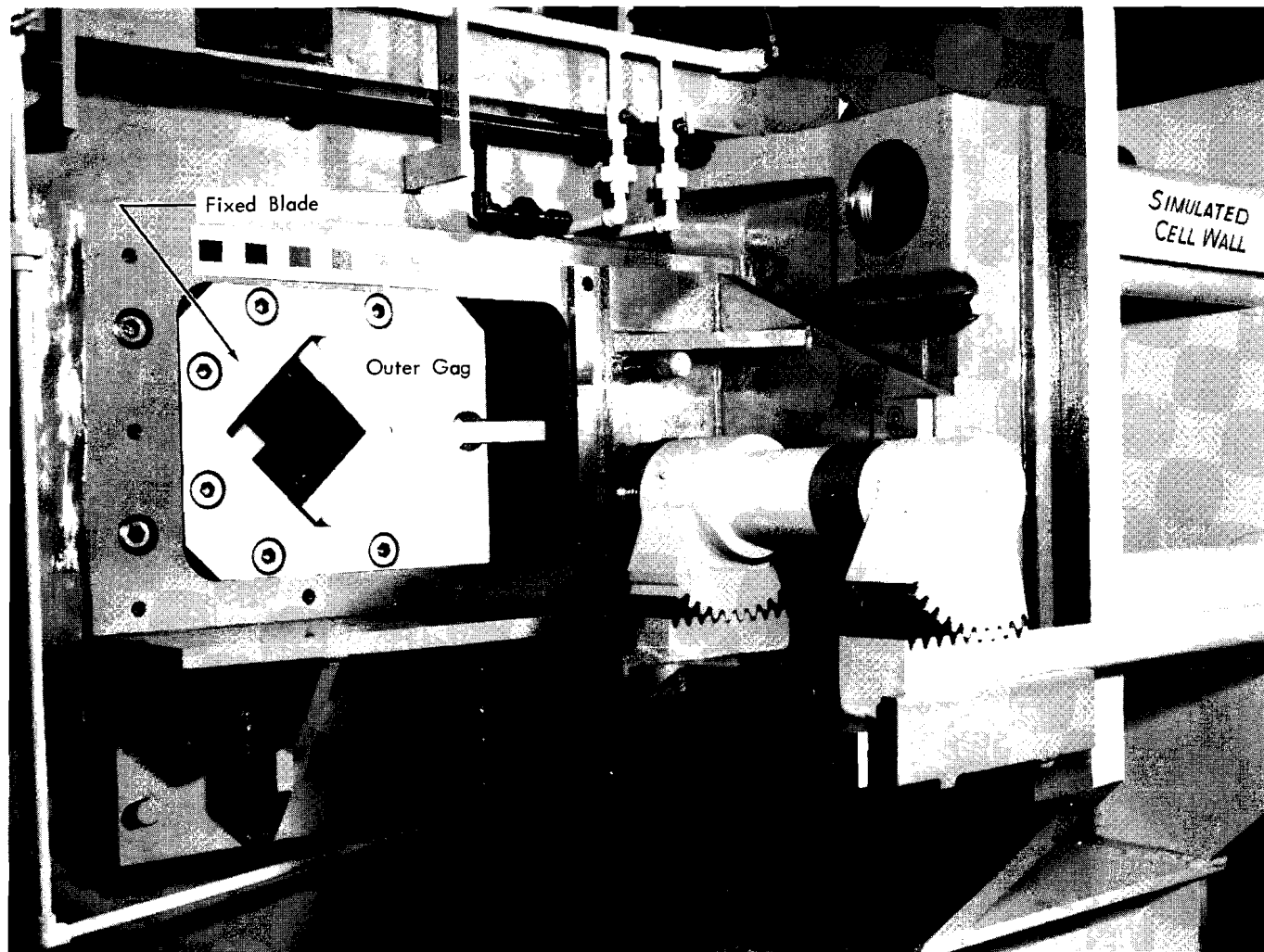


Fig. 3.7. View of 250-ton prototype shears showing fixed blade and outer gag.

Sheared product obtained from shearing a porcelain filled ORNL Mark I prototype fuel assembly is shown in Figure 3.8. The product consists of short sections of porcelain filled stainless steel, porcelain fines, end pieces with stainless steel plugs, flattened ferrules, and magnetic stainless steel fines.

The conveyor-feeder has been fabricated and assembled. It will be installed in Cell 1 of Bldg. 4505 and checked out using batches of chopped porcelain filled stainless steel.

Tests have been concluded on the leacher rotary drum using 1-in. sections of stainless steel rod and it was concluded that there is essentially no back mixing when using 2.5 liter batches. Additional tests will be conducted using chopped sections of porcelain filled stainless steel and water to simulate acid to study the behavior of the leacher when feeding both solids and liquids.

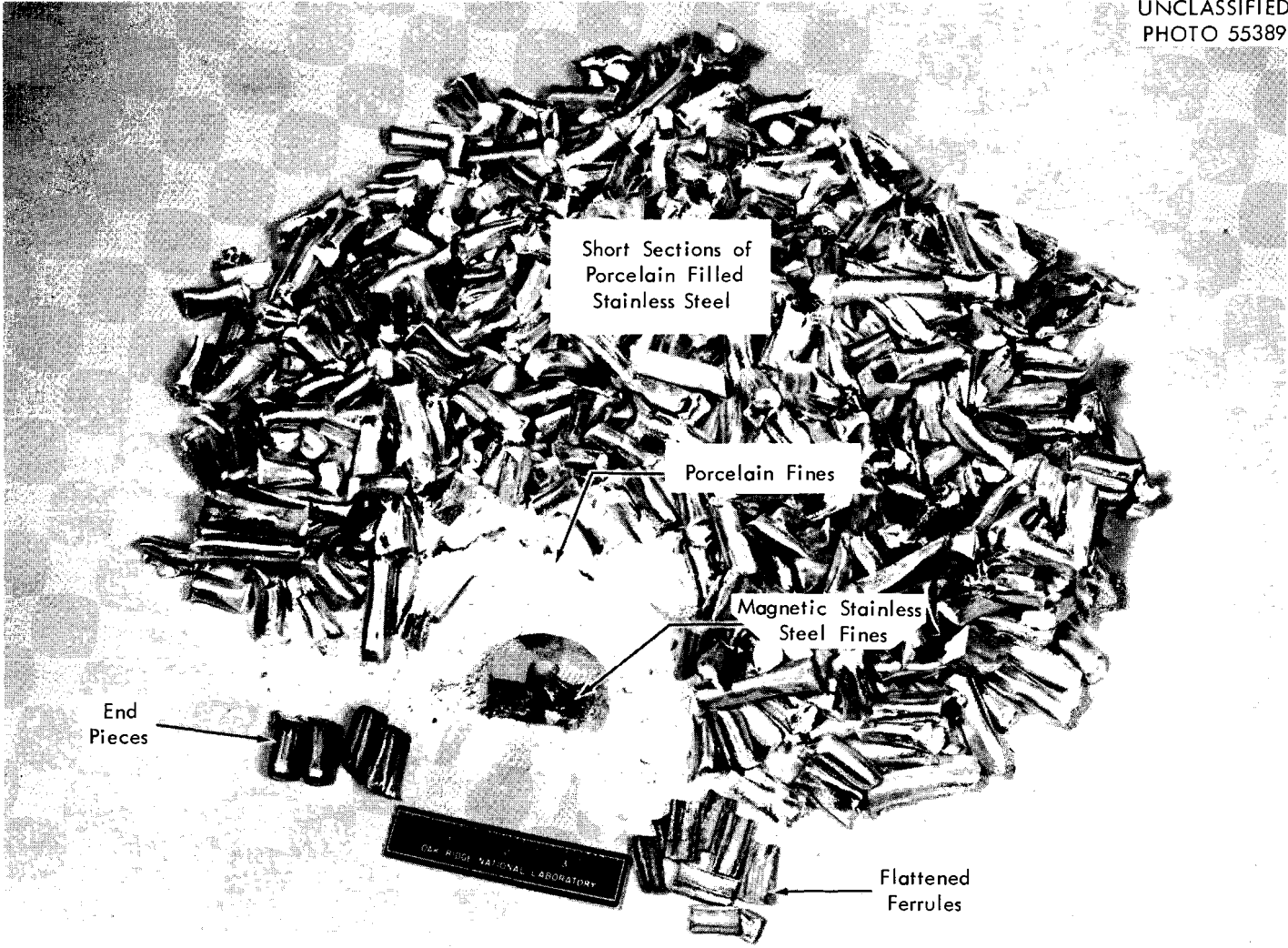


Fig. 3.8. Various type of material obtained when shearing porcelain filled Mark I prototype fuel assembly.

4.0 REACTOR EVALUATION STUDIES

J. C. Suddath

4.1 Heat Transfer from Spent Reactor Fuels during Shipping - J. S. Watson

After completing a series of temperature measurements with a 12-in.-ID x 2 ft simulated horizontal shipping cast and bundles containing up to 64 tubes of mock spent fuel pins, the cast was inverted and measurements started in the vertical position. Tables 4.1 through 4.4 show temperatures measured at a cross section at the midpoint in the bundle (12 in. from the bottom) with various heat generation rates. The center tube temperatures are very near those observed in the horizontal position. The surrounding tube temperatures are symmetrical but average very nearly the same as in the horizontal measurements. Shown along with the data are temperatures calculated with the procedure described in the Unit Operations Monthly Progress Report, June 1961. Here it is obvious that these approximate radiation calculations are optimistic at least near the outside of the bundle. It may be noted that the predicted temperatures near the center of the bundle are still reasonably good. It appears that all conservative or safety features in the radiation calculations within the bundle as well as convective effects are almost exactly balanced by the optimistic errors involved in calculating the temperatures in the outside tubes of the bundle.

In the horizontal position there was a significant amount of convective heat transfer demonstrated by the nonsymmetrical temperatures measured. However, because precise evaluation of the radiative and conductive fluxes have not yet been made, the relative effects of convection have not been assessed. With the bundle in the vertical position, the effects of convective currents should be noted from variations in the measured temperatures up the bundle. This effect can be seen in Tables 4.4 through 4.6 where temperature distributions measured at three positions up the bundle (12, 15, and 18 in. from the bottom) but with the same heat generation rate of 0.012 watts/cm are shown. The temperatures increased approximately 7°C over this range. The temperatures in the bundle will be highest at the very top of the cast, and probably longer casts would give higher maximum temperatures. However, obviously the bundle temperatures can not increase without limit since radiation and conduction will eventually be capable of transferring all of the generated heat from the bundle.

Table 4.1. Temperature Distribution in 64 Tube Vertical Bundle
at the Midpoint

1-1	1-2	1-3	1-4	1-5	1-6	1-7	1-8
86.80	100.0	<u>119.5</u>	<u>120.5</u>	<u>124</u>	<u>123</u>	<u>113.5</u>	<u>108</u>
		107.15	110.31	110.31	107.15	100.00	86.80
2-1	2-2	2-3	2-4	2-5	2-6	2-7	2-8
100.00	119.38	<u>127</u>	<u>130</u>	<u>131</u>	<u>130</u>	<u>117</u>	<u>68</u>
		129.95	134.58	134.58	129.95	119.38	100.00
3-1	3-2	3-3	3-4	3-5	3-6	3-7	3-8
<u>117</u>	<u>128.5</u>	<u>135</u>	<u>147.5</u>				
107.15	129.95	142.44	147.94	147.94	142.44	129.95	107.15
4-1	4-2	4-3	4-4	4-5	4-6	4-7	4-8
<u>117</u>	<u>133</u>	<u>143</u>					
110.31	134.58	147.94	153.84	153.84	147.94	134.58	110.31
5-1	5-2	5-3	5-4	5-5	5-6	5-7	5-8
110.31	134.58	<u>141</u>	<u>144</u>	<u>145</u>	<u>144</u>	<u>98</u>	<u>119</u>
		147.94	143.84	153.84	147.94	134.58	110.31
6-1	6-2	6-3	6-4	6-5	6-6	6-7	6-8
107.15	129.95	<u>137</u>	<u>140</u>	<u>142</u>	<u>138.5</u>	<u>128</u>	<u>119.5</u>
		142.44	147.94	147.94	142.45	129.96	107.15
7-1	7-2	7-3	7-4	7-5	7-6	7-7	7-8
100.00	119.38	129.95	134.58	<u>130.5</u>	<u>124</u>	<u>119</u>	<u>108.5</u>
				134.58	129.96	119.39	100.01
8-1	8-2	8-3	8-4	8-5	8-6	8-7	8-8
86.80	100.00	107.15	110.31	<u>120</u>	<u>119</u>	<u>108</u>	<u>102.5</u>
				110.31	107.15	100.01	86.80

Heat generation rate 0.02158 watts/tube-cm

Average wall temperature 53.0°C

(Measured temperatures are boxed and calculated temperatures open.)

Table 4.2. Temperature Distribution in 64 Tube Vertical Bundle
at the Midpoint

1-1	1-2	1-3	1-4	1-5	1-6	1-7	1-8
		155	156	162	160	148	139
110.05	126.94	135.95	139.91	139.91	135.95	126.94	110.05
2-1	2-2	2-3	2-4	2-5	2-6	2-7	2-8
		166	170	170.5	169.5	153	83
126.94	151.18	164.18	169.83	169.83	164.18	151.18	126.94
3-1	3-2	3-3	3-4	3-5	3-6	3-7	3-8
153	169	176.5	192				
135.95	164.18	179.37	186.00	186.00	179.37	164.18	135.95
4-1	4-2	4-3	4-4	4-5	4-6	4-7	4-8
154	174.5	188					
139.91	169.83	186.00	193.10	193.10	186.00	169.83	139.91
5-1	5-2	5-3	5-4	5-5	5-6	5-7	5-8
		184	189	190	188.5	125	156
139.91	169.83	186.00	193.10	193.10	186.01	169.83	139.91
6-1	6-2	6-3	6-4	6-5	6-6	6-7	6-7
		180	184	186	180.5	168	156
135.95	164.18	179.37	186.00	186.01	179.37	164.18	135.95
7-1	7-2	7-3	7-4	7-5	7-6	7-7	7-8
				170.5	162	155	140.5
126.94	151.18	164.18	169.83	169.83	164.18	151.19	126.95
8-1	8-2	8-3	8-4	8-5	8-6	8-7	8-8
				157	155.5	141	132
110.05	126.94	135.95	139.91	139.91	135.95	126.95	110.05

Heat generation rate 0.0337 watts/tube-cm

Average wall temperature 64.6°C

(Measured temperatures are boxed and calculated temperatures open.)

Table 4.3. Temperature Distribution in a 64 Tube Vertical Bundle
at the Midpoint

1-1	1-2	1-3	1-4	1-5	1-6	1-7	1-8
		196	198	206	203	187	177
135.00	154.98	165.53	170.15	170.15	165.53	154.99	135.00
2-1	2-2	2-3	2-4	2-5	2-6	2-7	2-8
		211	217	218	216	194	98
154.98	183.24	198.22	204.71	204.71	198.22	183.24	154.99
3-1	3-2	3-3	3-4	3-5	3-6	3-7	3-8
194	216	226.5	244.5				
165.53	198.22	215.63	223.20	223.20	215.63	198.22	165.54
4-1	4-2	4-3	4-4	4-5	4-6	4-7	4-8
197	223	240					
170.15	204.71	223.20	231.28	231.28	223.20	204.71	170.15
5-1	5-2	5-3	5-4	5-5	5-6	5-7	5-8
		235.5	242	241.5	240.5	160	199
170.15	204.71	223.20	231.28	231.28	223.20	204.71	170.15
6-1	6-2	6-3	6-4	6-5	6-6	6-7	6-7
		230	235	242.5	235	217	200
165.53	198.22	215.63	223.20	223.20	215.63	198.23	165.54
7-1	7-2	7-3	7-4	7-5	7-6	7-7	7-8
				218.5	206.5	198	180
154.99	183.24	198.22	204.71	204.71	198.23	183.24	154.99
8-1	8-2	8-3	8-4	8-5	8-6	8-7	8-8
				200.5	199	179	168
135.00	154.99	165.54	170.15	170.15	165.54	154.99	135.00

Heat generation rate 0.04852 watts/tube-cm

Average wall temperature 79.4°C

(Measured temperatures are boxed and calculated temperatures open.)

Table 4.4. Temperature Distribution in a 64 Tube Vertical Bundle
at the Midpoint

1-1	1-2	1-3	1-4	1-5	1-6	1-7	1-8
		84	86	88	86.5	80.5	77
63.50	72.69	77.76	80.02	80.02	77.76	72.69	63.50
2-1	2-2	2-3	2-4	2-5	2-6	2-7	2-8
		89	91	92	91.5	82.5	52.5
72.69	86.60	94.37	97.81	97.81	94.37	86.60	72.69
3-1	3-2	3-3	3-4	3-5	3-6	3-7	3-8
83	90	94	102.5				
77.76	94.37	103.70	107.86	107.86	103.71	94.37	77.76
4-1	4-2	4-3	4-4	4-5	4-6	4-7	4-8
83	93	99.5					
80.02	97.81	107.86	112.35	112.35	107.86	97.82	80.03
5-1	5-2	5-3	5-4	5-5	5-6	5-7	5-8
		98	100.5	101	100	71	85
80.03	97.81	107.86	112.35	112.35	107.86	97.82	80.03
6-1	6-2	6-3	6-4	6-5	6-6	6-7	6-8
		96.5	98	99	96.5	90	85
77.76	94.37	103.71	107.86	107.86	103.71	94.38	77.76
7-1	7-2	7-3	7-4	7-5	7-6	7-7	7-8
				92	87	85	78
72.69	86.60	94.37	97.82	97.82	94.38	86.60	72.69
8-1	8-2	8-3	8-4	8-5	8-6	8-7	8-8
				85	85	78	74.5
63.50	72.69	77.76	80.03	80.03	77.76	72.69	63.50

Heat generation rate 0.01212 watts/cm

Average wall temperature 41.2°C

(Measured temperatures are boxed and calculated temperatures open.)

Table 4.5. Temperature Distribution in a 64 Tube Vertical Bundle

15 in. from the Bottom

1-1	1-2	1-3 79.5	1-4 82	1-5 83	1-6 82	1-7 77.5	1-8 72
2-1	2-2	2-3 89.5	2-4 91	2-5 91	2-6 90.5	2-7 84	2-8 50
3-1 79	3-2 92.5	3-3 96	3-4 99.5	3-5	3-6	3-7	3-8
4-1 80.5	4-2 94.5	4-3 100.5	4-4 101.5	4-5	4-6	4-7	4-8
5-1	5-2	5-3 100.5	5-4 101	5-5 101.5	5-6 98	5-7 91	5-8 80.5
6-1	6-2	6-3 97	6-4 99	6-5 100	6-6 98	6-7 90	6-8 81
7-1	7-2	7-3	7-4	7-5 90.5	7-6 89.5	7-7 87	7-8 77
8-1	8-2	8-3	8-4	8-5 80	8-6 81.5	8-7 78	8-8 71.5

Heat generation rate 0.01212 watts/tube-cm
 Average wall temperature 37.4°C

Table 4.6. Temperature Distribution in a 64 Tube Vertical Bundle
18 in. from the Bottom

1-1	1-2	1-3 86	1-4 87	1-5 88.5	1-6 87	1-7 81.5	1-8 76
2-1	2-2	2-3 93	2-4 96	2-5 97	2-6 95.5	2-7 88	2-8 81
3-1 84	3-2 96	3-3 103	3-4 106	3-5	3-6	3-7	3-8
4-1 82	4-2 98	4-3 106	4-4 109	4-5	4-6	4-7	4-8
5-1	5-2	5-3 105	5-4 106	5-5 107	5-6 104	5-7 96	5-8 85
6-1	6-2	6-3 104	6-4 104	6-5 104	6-6 102	6-7 94	6-8 85
7-1	7-2	7-3	7-4	7-5 96	7-6 94	7-7 92	7-8 82
8-1	8-2	8-3	8-4	8-5 88	8-6 86	8-7 82	8-8 76

Heat generation rate 0.01212 watts/tube-cm
 Average wall temperature 41.0°C

5.0 VOLATILITY

R. W. Horton

5.1 Sorption of UF_6 on NaF - L. E. McNeese

Determination of the factors which control the rate of removal of UF_6 from a flowing gas stream by a fixed bed of NaF has been the subject of a number of recent studies. To date, no physical model has been set forth which adequately explains the observed characteristics of the sorption phenomenon. These characteristics will be reviewed after which a possible model will be discussed. Equations based on this model will be derived and preliminary solutions discussed.

Characteristics of the Sorption Phenomenon. The sorption of UF_6 by NaF was first reported by Martin, et al,¹ who observed the formation of a lemon-yellow product in which the molar ratio of UF_6 to NaF was 0.333 whereupon it was concluded that a complex having the formula $UF_6 \cdot 3NaF$ was formed. Sorption was carried out at 20-120°C and it was observed that desorption could be effected by raising the temperature to 400°C. Subsequent study by Cathers, et al,² of the formation and decomposition reactions of the complex showed that the dissociation pressure of UF_6 above the complex was a function of temperature only, and was expressible as $\log P = A + B/T^\circ K$. The dissociation pressure is only 1 mm Hg at 195°C. The dissociation pressure was notably independent of the fractional conversion of NaF to complex in a sample. The sorption reaction was observed to be reasonably exothermic (-23.2 kcal/mole UF_6). The first rate studies were those of Worthington³ who measured the rate of sorption of pure UF_6 at 56 mm Hg pressure on finely divided NaF powder in the temperature range 80-130°C. The fractional conversion was observed to depend on time in a logarithmic manner, with fractional conversion increasing with an increase in temperature at a constant reaction time. The product of the reaction was observed to be $UF_6 \cdot 3NaF$.

Subsequent rate studies were carried out by Massoth and Hensel⁴ on NaF powder, pellets, and crushed pellets using pure UF_6 at 90 mm Hg in the temperature range 24-68°C. The reaction rate for the powder was observed to follow the parabolic rate law, i.e.

$$\frac{dx}{dt} = \frac{k}{x}$$

x = thickness of product film due to partial reaction

t = time

k = constant

The reaction with crushed pellets followed the logarithmic rate law, $\frac{dx}{dt} = ae^{-bx}$ initially but after ~200 sec followed the parabolic rate law. The sorption rate was observed to depend inversely on the particle size.

The reaction of UF_6 with NaF pellets produced results quite different to those observed for the powder or crushed pellets. The reaction was observed to proceed rapidly at first and then to apparently stop at $\sim 40\%$ conversion. A small inverse effect of temperature upon extent of reaction was noted. A physical blockage due to buildup of complex on the outside of the pellet was suggested as an explanation of the incomplete reaction. No explanation of the inverse temperature effect was given.

Recent studies in the Unit Operations Section on the removal of UF_6 from a flowing UF_6-N_2 stream by a fixed bed of NaF pellets have in general substantiated most of the characteristics noted by the previous investigations. Notably, the effects of strong inverse temperature dependence of the rate and extent of reaction over the range $30-125^\circ C$ have been observed.

In summary, it may be concluded that a complex of the formula $UF_6 \cdot 3NaF$ is formed by a chemisorption reaction. Reasons for this conclusion are:

1. Non-dependence of dissociation pressure on extent of conversion.
2. Magnitude of heat sorption.
3. Color change due to reaction.

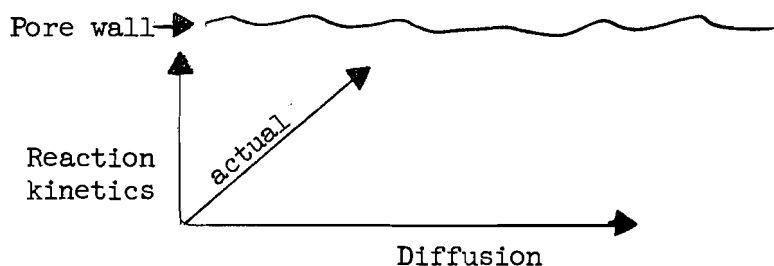
From the rate studies on powder and crushed pellets of NaF, the effect of an increase in temperature is that of increasing the local rate of sorption. It is probable that this is true in the case of pellets, and that some mechanism other than kinetics is responsible for the inverse temperature effect.

In attempting to explain the temperature effect, one can rule out large temperature gradients in the solid; the maximum temperature difference between the inside of the pellet and the surface is of the order of $1^\circ C$ or possibly much less. Therefore, the effect can not be due to dissociation pressure which is only 1 mm Hg at $195^\circ C$.

One can also observe that the sorbed UF_6 is concentrated around the periphery of the NaF pellet, and that the center appears completely unconverted. It is also evident that the rate of reaction between UF_6 and a clean NaF surface is quite fast, but that appreciable resistance to reaction is afforded by a film of the complex.

Model of Sorption Process. In choosing a model to represent a physical system, one invariably attempts to contrive a simplified picture of reality, which nevertheless must satisfy and account for the observed characteristics of reality.

The present model is based on a very simple idea. Consider the movement of gaseous UF_6 in an open pore within the NaF pellet. One force contributing to the movement is that of Fickian diffusion along the gas phase concentration gradient. If the NaF at the pore walls is not completely reacted, there will also be a net movement toward the pore wall due to reaction of UF_6 at the wall. One can visualize these two forces as vectors



and obtain the magnitude and relative direction of movement of UF_6 into the NaF pellet. An increase in temperature will cause an increase in the magnitude of both the diffusion vector and the reaction kinetics vector; however, not by the same relative amount. Since the diffusivity varies as $T^{3/2}$ and the rate constant as $\frac{A}{RT} e^{-\frac{E}{RT}}$

a change in temperature will cause a larger relative change in the reaction kinetics vector than in the diffusion vector. Thus the magnitude of the actual movement will become greater, but more important, the direction of the actual movement will become more nearly toward the pore wall. This is the expected result and represents nothing new.

Measurements of the crystalline density of the complex indicate that the open pore volume in a NaF pellet would be filled with complex before complete conversion of the NaF. It is with this condition that the relative movement and direction of the UF_6 in the pores becomes important. The apparent sorption capacity is directly related to the direction of the actual movement of UF_6 . For, if the diffusivity were infinite compared to the rate of reaction at the pore wall, the UF_6 concentration in the pores throughout the pellet would be constant and when the pores at the pellet surface became filled with complex, as also would the pores at the center of the pellet. The point-to-point conversion of NaF to complex would be invariant and one would observe the maximum fractional conversion of NaF to complex. If, on the other hand, the rate of reaction at the pore wall were infinite when compared to the rate of diffusion along the pore, the pores at the surface would become filled whereas those at the center would be completely unreacted. One would observe an infinitesimally thin layer of complex-filled pores around the periphery of the pellet and the average fractional conversion of NaF in the pellet to complex would be infinitesimal. Clearly, this would represent the case of minimum fractional conversion. The tacit assumption has been made in the foregoing that the rate of diffusion of UF_6 through the solid phase is negligible when compared to the rate through the open pores in the pellet.

Thus, the present model accounts for the inverse temperature effect and yet retains the actual kinetic characteristics of the system as shown by studies with NaF powder and crushed pellets. The characteristics of the sorption rate becoming negligible before complete conversion is also explained as in the physical appearance of the reacted pellet.

Derivation of Equations. Prior to the derivation of the partial differential equations for the system, one must write an expression for the local reaction rate within the pellet. There are at least two possible relations which should be considered. The first is of the form

$$r = a \rho_{\text{NaF}} S e^{-bx} C \gamma$$

where

r = reaction rate, g moles UF_6 /sec-cm³ pellet

a = constant, $\frac{\text{g moles } \text{UF}_6}{\text{sec-cm}^2 \text{ internal area}} \frac{\text{g mole } \text{UF}_6}{\text{g mole gas}}$

S = internal surface area, cm²/g pellet

ρ_{NaF} = pellet density, g/cm³ pellet

x = film thickness of product, cm

b = constant, cm⁻¹

C = UF_6 concentration in open pore space, g moles UF_6 /g mole gas

γ = ratio, internal surface area/original internal surface area

The second relation is of the form

$$r = \frac{a' \rho_{\text{NaF}} S C \gamma}{b' + x}$$

where

a' = constant, $\frac{\text{g moles } \text{UF}_6\text{-cm film thickness}}{\text{sec-cm}^2 \text{ internal area}} \frac{\text{g mole } \text{UF}_6}{\text{g mole gas}}$

b' = constant, cm film thickness

The quantities, a , b , a' , and b' , are functions of temperature.

The difference between the two rate equations lies in the effect of product film thickness. The second case is simply that of slab conduction and considers the product layer to be integral. The first case has been observed when the reaction product film cracks so as to afford less resistance to diffusion of the reactant than would otherwise be expected. Thus far in the study, only the first case has been considered.

For convenience, β will be defined

$$\beta = a\rho_{\text{NaF}} \text{Se}^{-bx} \gamma$$

so that the reaction rate equation becomes

$$r = \beta C$$

Before proceeding further with the derivation, one must find the variation of γ with fractional conversion, and one must find the variation of the open void volume α with fractional conversion.

Although one is dealing with NaF pellets which are 1/8-in. right circular cylinders, in order to simplify the system it will be assumed that one is dealing with a sphere having the same volume as a pellet. The external surface area of this sphere is 11.4% less than that of the cylinder.

Consider a sphere of NaF of volume $V \text{ cm}^3$ and weight W grams. The surface area per unit weight will be $S \text{ cm}^2/\text{g}$. If the theoretical density of NaF is $\rho_{\text{th}} \text{ g/cm}^3$, then the fraction of the volume V which is void is

$$1 - \frac{W}{V\rho_{\text{th}}}$$

Let f represent the fraction of this void volume which is open, i.e. connected with the external surface. It will be assumed that the internal surface area SW bounds the effective void volume

$$Vf \left(1 - \frac{W}{V\rho_{\text{th}}} \right)$$

Assume that the distribution of effective void volume is homogeneous and consider a unit area from a spherical shell of thickness $\Delta r \text{ cm}$. The unit area can be flattened into a slab of thickness $\Delta r \text{ cm}$ which will contain an effective void volume of $f(1 - W/V\rho_{\text{th}})$. Assume that this volume is taken up by N cylinders of length Δr and diameter $\delta \text{ cm}$.

Then

$$f \left(1 - \frac{W}{V\rho_{\text{th}}} \right) = \frac{\pi}{4} \delta^2 \Delta r N$$

Associated with the element of thickness Δr is the internal surface area of

$$S \frac{W}{V}$$

If the above N cylinders have this surface area, then

$$S \frac{W}{V} = \pi \delta \Delta r N$$

Dividing the two relations, one has

$$\frac{f \left(1 - \frac{W}{V \rho_{th}} \right)}{\left(S \frac{W}{V} \right)} = \frac{\frac{\pi}{4} \phi^2 \Delta r N}{\pi \delta \Delta r N}$$

or

$$\delta = \frac{4f}{S} \left[\frac{1}{\rho} - \frac{1}{\rho_{th}} \right]$$

Thus, one has assumed that the totality of the open void volume of the pellet is contained in pores of diameter δ cm.

In a straight forward manner, one can show that the maximum fractional conversion of NaF to complex in a pellet which retains its original dimensions is

$$\text{frac sat} = \frac{1 - \frac{\rho_c}{\rho_{NaF}} \frac{126}{478} \left[1 - f \left(1 - \frac{\rho_{NaF}}{\rho_{th}} \right) \right]^{-1}}{\frac{\rho_{th}}{f(\rho_{th} - \rho_{NaF})} - 1}$$

where

ρ_c = density of complex, g/cm³

ρ_{NaF} = density of original pellet, g/cm³

ρ_{th} = theoretical density of NaF = 2.79 g/cm³

f = fraction of void volume which is connected to external surface

Similarly, α , the ratio

$$\frac{\text{open void volume}}{\text{total volume}}$$

may be expressed as

$$\alpha = f \left(1 - \frac{\rho_{NaF}}{\rho_{th}} \right) \left\{ 1 - F - \frac{F \rho_{th}}{f(\rho_{th} - \rho_{NaF})} \left[\frac{478}{126} \frac{\rho_{NaF}}{\rho_c} - 1 \right] \right\}$$

The film thickness of complex as a function of fractional conversion F can be expressed as

$$\text{film thickness} = \frac{4f(\rho_{th} - \rho_{NaF})}{S \rho_{NaF} \rho_{th}} \left[\left\{ 1 + F \left(\frac{\rho_{th}}{f(\rho_{th} - \rho_{NaF})} - 1 \right) \right\}^{1/2} - \left\{ \frac{F\rho_{th}}{f(\rho_{th} - \rho_{NaF})} \left(1 - \frac{478}{126} \frac{\rho_{NaF}}{\rho_c} \right) - F + 1 \right\}^{1/2} \right]$$

Also, γ , the ratio internal surface area/orig int. surface area can be obtained from the film thickness and the expression for δ , the original pore diameter, by using a log mean average of the internal and external diameters of the reacted zone as shown in Figure 5.1. The relation is

$$\gamma = \frac{\left\{ 1 + F \left(\frac{\rho_{th}}{f(\rho_{th} - \rho_{NaF})} - 1 \right) \right\}^{1/2} - \left\{ \frac{F\rho_{th}}{f(\rho_{th} - \rho_{NaF})} \left(1 - \frac{478}{126} \frac{\rho_{NaF}}{\rho_c} \right) - F + 1 \right\}^{1/2}}{\ln \frac{\left[1 + F \left(\frac{\rho_{th}}{f(\rho_{th} - \rho_{NaF})} - 1 \right) \right]^{1/2}}{\left[\frac{F\rho_{th}}{f(\rho_{th} - \rho_{NaF})} \left(1 - \frac{478}{126} \frac{\rho_{NaF}}{\rho_c} \right) - F + 1 \right]^{1/2}}}$$

One can now proceed with the main derivation, i.e., the relation specifying the concentration C of unreacted UF_6 in the open pore volume as a function of radial position and time.

Consider a spherical shell of thickness Δr cm with inner radius r cm and outer radius $(r + \Delta r)$ cm as shown in Figure 5.2.

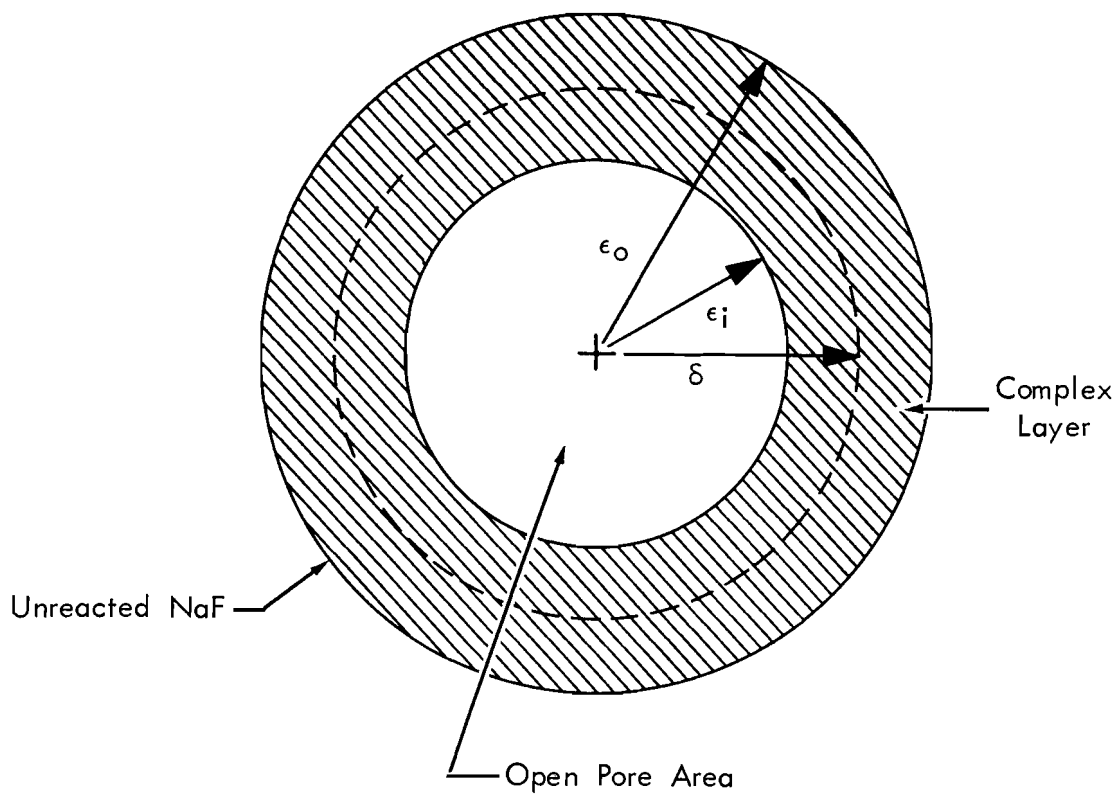
Spherical symmetry will be assumed. At the radial position r, the concentration of unreacted UF_6 in the open void volume will be taken as C g moles UF_6 /g mole gas and the fraction of the total volume which is open void volume will be taken as $\alpha(r)$. Then, at the radial position $(r + \Delta r)$ the concentration will be $C + \partial c/\partial r \Delta r$ and the fraction of the total volume which is open and void will be $\alpha(r) + \alpha'(r)\Delta r$.

The open void volume in the shell is then

$$\text{open void volume} = 4\pi r^2 \Delta r \left[\alpha(r) + \alpha'(r) \frac{\Delta r}{2} \right]$$

Since the medium is assumed to be homogeneous, the ratio of open area to total area at $(r + \Delta r)$ is

UNCLASSIFIED
ORNL-LR-DWG 65314



$$\gamma = \frac{\epsilon_0 - \epsilon_i}{\ln \frac{\epsilon_0}{\epsilon_i}}$$

Fig. 5.1. Diameters used for obtaining γ .

UNCLASSIFIED
ORNL-LR-DWG 65315

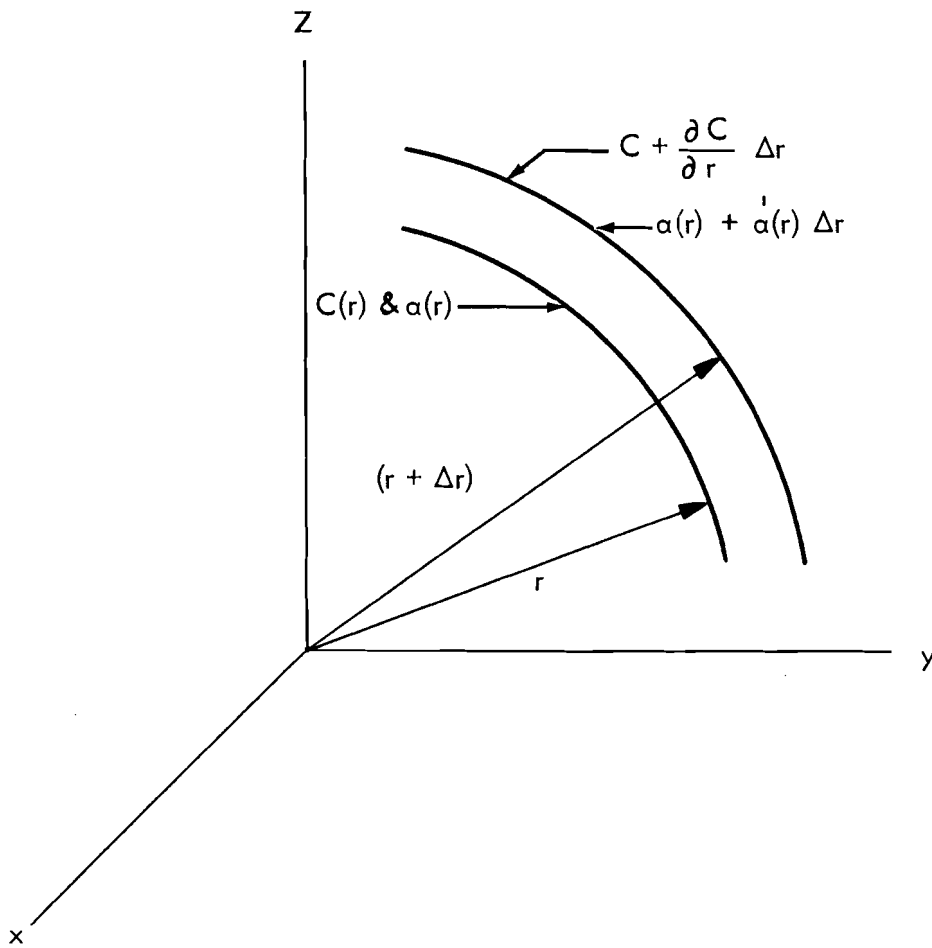


Fig. 5.2. Typical spherical shell.

$$\alpha(r) + \alpha'(r) \Delta r$$

Thus the rate of diffusion of UF_6 into the shell is

$$\text{rate in, } \frac{\text{g moles } UF_6}{\text{sec}} = 4\pi(r + \Delta r)^2 \left[\alpha(r) + \alpha'(r) \Delta r \right] D' \frac{\partial(c + \frac{\partial c}{\partial r} \Delta r)}{\partial r}$$

where

D' = effective diffusivity of UF_6 through the open pore volume,
g moles gas/sec-cm gas

It should be observed that D' will be a fraction of the value of the diffusivity of UF_6 in N_2 due to the elongated and partially blocked nature of the actual diffusion path. The value of D' would be the actual diffusivity only if all of the pores were aligned radially from the center of the sphere. Similarly, the rate of diffusion of UF_6 out of the shell is

$$\text{rate out, } \frac{\text{g moles } UF_6}{\text{sec}} = 4\pi r^2 \alpha(r) D' \frac{\partial c}{\partial r}$$

The rate of reaction of UF_6 within the shell is

$$\text{rate of reaction, } \frac{\text{g moles } UF_6}{\text{sec}} = 4\pi r^2 \Delta r \beta c$$

The rate of accumulation of unreacted UF_6 in the shell is

$$\text{rate of accumulation, } \frac{\text{g moles } UF_6}{\text{sec}} = 4\pi r^2 \Delta r \frac{\partial}{\partial t} \left\{ c \left[\alpha(r) + \alpha'(r) \frac{\Delta r}{2} \right] \right\} \frac{273}{22400T^\circ K}$$

Then, since

Rate of accumulation = Rate of diffusion in - Rate of diffusion out - Rate of reaction

$$4\pi r^2 \Delta r \frac{\partial}{\partial t} \left\{ \left[\alpha(r) + \alpha'(r) \frac{\Delta r}{2} \right] c \right\} \frac{273}{22400T^\circ K} =$$

$$4\pi(r + \Delta r)^2 \left[\alpha(r) + \alpha'(r) \Delta r \right] D' \frac{\partial(c + \frac{\partial c}{\partial r} \Delta r)}{\partial r} - 4\pi r^2 \alpha(r) D' \frac{\partial c}{\partial r} - 4\pi r^2 \Delta r \beta c$$

Dividing by $4\pi r^2 \Delta r$, and taking the limit as $\Delta r \rightarrow 0$, one obtains the fundamental equation governing the concentration of unreacted UF_6 in the pellet as a function of time and position:

$$\frac{\partial}{\partial t} (c\alpha) = D_e \alpha \left\{ \frac{\partial^2 c}{\partial r^2} + \left(\frac{2}{r} + \frac{\alpha'}{\alpha} \right) \frac{\partial c}{\partial r} \right\} - \beta c$$

where

D_e = effective diffusivity of UF_6 through N_2 in the pellet, cm^2/sec

It should be recalled that α and β are functions of the fractional conversion so that the equation has non-constant coefficients. Achievement of an analytical solution to the equation seems highly improbable. Thus, in order to integrate the equation over time and space, one must resort to a numerical solution.

After one obtains the solution of the relation for $C(r,t)$ one can use this to find the rate of loading of the pellet and the distribution of reacted UF_6 in the pellet.

The finite difference method of DuFort and Frankel⁵ has been used in order to allow a practical integration time for the system of finite difference relations. The finite difference equations were coded for solution on the IBM-7090 computer allowing for a film type resistance to mass transfer at the external surface of the sphere. The code was checked against Danckwerts'⁶ analytical solution for the equation

$$\frac{\partial C}{\partial t} = D \left\{ \frac{\partial^2 C}{\partial r^2} + \frac{2}{r} \frac{\partial C}{\partial r} \right\} - k C$$

where k and D are constants

Satisfactory convergence was observed.

Preliminary solutions of the system of equations have the observed characteristics of the experimental system. Loading curves for single layers of NaF pellets at constant temperature, flow rate, and UF_6 concentration will be used to test the model further and set values for the constants within it.

References

1. Martin, H., Albers, A., and Dust, H. P., "Double Fluorides of Uranium Hexafluoride," *Z. Anorg. Allg. Chemie* 265, 128-38 (1951).
2. Cathers, G. I., Bennett, M. R., and Jolley, R. L., "Formation and Decomposition Reactions of the Complex $UF_6 \cdot 3NaF$," ORNL CF 57-4-25.
3. Worthington, R. E., "The Reactions of Sodium Fluoride with Hex and Hydrogen Fluoride," IGR-R/CA-200.
4. Massoth, F. E., and Hensel, W. E., Jr., "Kinetics of the Reaction of Uranium Hexafluoride with Sodium Fluoride Powder, Pellets, and Crushed Pellets," GAT-230.
5. DuFort, E. C., and Frankel, S. P. "Stability Conditions in the Numerical Treatment of Parabolic Differential Equations," *Math. Tables Aides Comput.*, 7, 135-152 (1953).

6. Danckwerts, P. V., Trans. Faraday Soc. 47, 1014 (1951).

5.2 Dissolution of EBR-1 Core II Meltdown - W. W. Pitt, Jr.

The Volatility Pilot Plant has available for processing the residue of the stainless steel jacketed Core II from the EBR-1. Laboratory experiments and other studies indicate there should be no difficulties associated with the processing of this fuel with the exception of a possible violent reaction of NaK. Hence these studies were conducted to determine possible hazards presented by the NaK in the core residue.

The EBR-1 is a NaK cooled, solid fueled, fast breeder reactor with depleted U blanket. It was designed and built by Argonne National Laboratory and put into operation by ANL at the National Reactor Testing Station in Idaho in 1951.¹ Core II was a hexagonal array of 217, SS 347 tubes of 0.021-in. wall each containing two 0.384 diameter enriched uranium 2 wt % zirconium alloy fuel slugs 4-1/4-in. long; one 4-1/4-in. long lower blanket slug of stainless steel jacketed unenriched U-Zr alloy; and two, 3-3/4-in. long upper blanket slugs, also stainless steel jacketed unenriched U-Zr alloy. The 0.012-in. annulus was filled with NaK. Due to the economic advantage, the reactor was constructed of 347 stainless steel, even though it was known that uranium forms low-melting eutectics with iron, nickel, and chromium (three main constituents in stainless steel). On November 29, 1955, during experiments at high core temperatures and a short reactor period, a partial meltdown of the fuel occurred and damaged the core assembly.^{2,3}

After this incident and a reasonable decay time, the core was removed from the reactor and disassembly began. Disassembly was completed at the Lemont site of ANL.⁴ An artist's reconstruction, based on observations during disassembly, was made at ANL (Figure 5.3).⁴

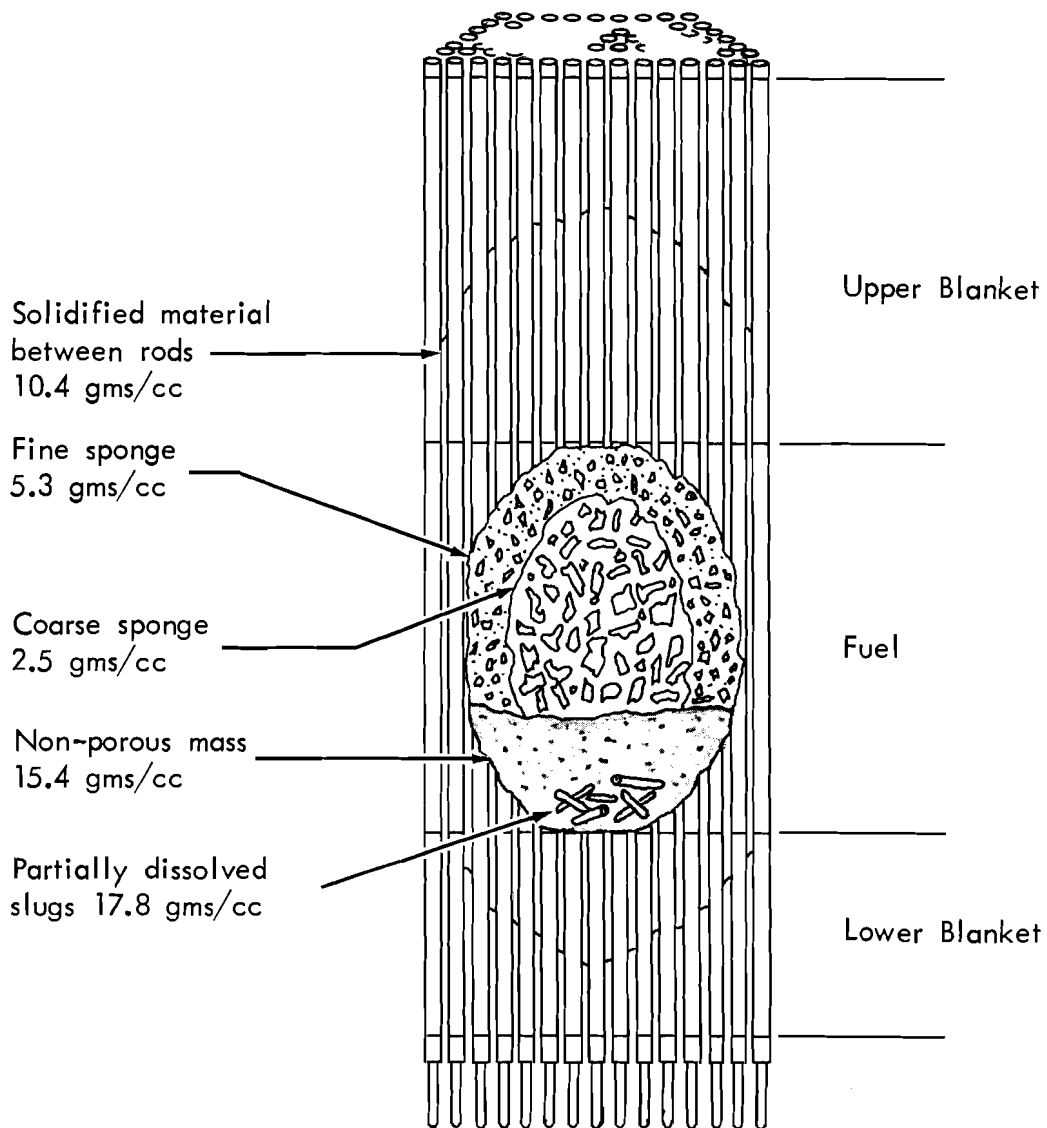
Present Condition of Core II Fuel. The material from the fuel section of the core exists as a nonhomogeneous mixture of stainless steel, uranium, zirconium, and NaK sealed in enameled steel cans 2-in. high by 3-in. dia. There are 105 of these cans containing various weights of material between 93 and 1100 g, with the average can containing ~1000 g. The weight of each filled can is an indication of the relative volume of NaK which might possibly be entrained (the heavier the can the less NaK entrained; Sp. G. NaK < 1, solids ~15).

NaK Considerations. It is the unknown quantity of NaK in the EBR-1 cans that causes concern whenever a paper study of processing these cans is made. Chemical analysis of samples from the meltdown indicated that some of the sponge like solid material contained as much as 35 vol % NaK, and possibly more.

The reaction of HF and NaK is very rapid and exothermic, but since it requires 2 moles of HF for each mole of H₂ evolved, there would be no pressure increase due to gas evolution. Since the vapor pressure of NaK at 1200°F is only 200 mm Hg, there would be no pressure increase due to vaporization of NaK. This leaves us with the possibility of an explosive

Reprinted from Argonne National Laboratory
Report ANL-5731, p. 68 (see Ref. 4)

UNCLASSIFIED
ORNL-LR-DWG 65316



Scale in. $\frac{0}{1}$

Fig. 5.3. Artist's reconstruction of a vertical cross section through the damaged EBR-I core. The most reliable values for the densities of the various areas are shown at the left.

type reaction, a rapid expansion of gases due to an extreme rise in temperature. While this might occur, it is extremely unlikely that more than a small fraction of large quantities of NaK will react instantaneously, due to the low surface to volume ratio or low quantity of HF available. For any reasonable reaction time, the 140 kcal evolved per g mole of NaK reacted, would be easily absorbed in the fused salt bath.

NaK Dissolution Experiment. A 6 in. length of 304 SS tubing of 10 mil wall thickness containing 8 cc of NaK was dissolved with HF in a fused salt bath. The vessel used was the 3.5 in. dia by 12 in. deep INOR-8 pot previously used for ZrO₂ dissolutions. The 4 kg of 26-42.5-31.5 mol % NaF-LiF-ZrF₄ salt was maintained at ~500°C for 4 hrs dissolution time and then raised to ~600°C for 4 hrs. The HF flow rate was 0.25 lb/hr. After 5 hrs of dissolution time a salt splash caused a partial plugging of the off-gas line and subsequent rise in vessel pressure. However after removal of the plug, the pressure returned to normal, and HF flow was resumed and continued for 3 more hrs. Though there is no way of knowing when the SS tube was penetrated, it is believed this occurred at the time of the salt splash. It is known that the SS was not penetrated at the end of 4 hrs and no trace of the tube was found after 8 hrs. The 5 hr dissolution time for the tube corresponds to the 2 mil/hr rate reported for 304 SS. The salt splash was probably caused by the evolution of a large quantity of H₂ from the NaK and HF reaction, though there was not enough to give a noticeable pressure increase. There also was no increase in salt temperature due to the exothermic reaction.

While this one experiment is not conclusive, it does indicate that the entrained NaK is not likely to produce an explosive reaction during dissolution of the EBR-1 can by HF in fused salt.

References

1. H. V. Lichtenberger, et al., "Operating Experience and Experimental Results Obtained from a NaK-Cooled Fast Reactor," Proc. Int. Conf. on the Peaceful Uses of Atomic Energy, (United Nations, New York, 1955), Vol. 3, pp. 345-360.
2. W. H. Finn, "A Letter on EBR-1 Fuel Meltdown," Nucleonics, 14, No. 6, 35 (1956).
3. R. O. Brittan, "The EBR-1 Meltdown - Analysis of the Incident," ANL-5756.
4. J. H. Kittel, M. Novick, and R. T. Buchanan, "The EBR-1 Meltdown - Physical and Metallurgical Changes in the Core," ANL-5731.

6.0 WASTE PROCESSING

J. C. Suddath

The purpose of the waste processing program is to develop equipment and produce design data suitable for the final design of a waste calcination pilot plant. Test R-41, reported this month, was a Ca-Purex calcination test.

6.1 Evaporator-Calciner Test R-41 - C. W. Hancher

Evaporator-calciner test R-41 was a Purex calcination with calcium added to decrease sulfate volatility. When $\text{Ca}(\text{OH})_2$ is added to Purex feed the resulting CaSO_4 slurry is difficult to handle because it settles fast and tends to plug feed lines.

Calcium is better than Na or Mg for decreasing sulfate volatility because the resulting CaSO_4 is more stable, and operating experiences show less internal corrosion of the calciner vessels. Therefore, Ca was used and was added directly to the calciner in the form of $\text{Ca}(\text{NO}_3)_2$ because a soluble additive was easier to handle.

Calcium nitrate was prepared by dissolving $\text{Ca}(\text{OH})_2$ (hydrated lime) in concentrated HNO_3 (slowly). The resulting 3 to 4 molar solution was an ideal additive. In a plant operation the recycle nitric acid from the distillation column could be used to make up the $\text{Ca}(\text{NO}_3)_2$. $\text{Ca}(\text{NO}_3)_2$ was added through the extra liquid level probe line into the calciner pot. About 50% of $\text{Ca}(\text{NO}_3)_2$ was precharged to the calciner pot before the test was started. The remaining 50% was added at a fixed continuous rate throughout the test. A CPS-1-3/8 in. piston lapp pump was used to feed the $\text{Ca}(\text{NO}_3)_2$ to the calciner pot.

6.2 Test Results

Test R-41 calcination of Purex waste (Table 6.1) with calcium was not completely successful. The system was just about in control one hour after start-up when there was a plant wide evacuation drill, Table 6.2. The system was completely shutdown and started up 20 min later. This shutdown period caused a number of difficulties, the major difficulty being that the calciner liquid level probes plugged a number of times during the remainder to the feeding period, however, 391 liters of feed went into the system in 6 hrs, which gave the high average feed rate of 65 liter per hour (Tables 6.3 and 6.4 and Figure 6.1). The usual rate is 20-25 liters per hour. The material balances for the test were not satisfactory:

Nitrate	108% (this about correct)
Iron	78% (low)
Sulfate	67% (low)
Ruthenium	61% (low)

Table 6.1. R-41 Feed Concentration

	H molar	HNO ₃ molar	Fe g/l	Na g/l	SO ₄ g/l	Ru g/l
As madeup	5.1	6.1	25.0	13.1	96.0	0.15
As analyzed						
Tank 1	5.38	6.17	27.5	12.8	104.0	0.110
Tank 2	5.26	5.91	27.5	12.4	94.9	0.126

Table 6.2. Test R-41 Operation Log

8:00 a.m.	Precharge Ca(NO ₃) ₂ ~20 liters of 3 M
9:00	Evaporator full - calciner heat on, start to fill calciner
9:20	Calciner liquid up to operating level
10:00	Shutdown - Laboratory evacuation drill
10:20	Start-up after drill
3:30 p.m.	Feed all in system
5:00	Evaporator on standby
10:00 a.m.	Stopped calcining

Table 6.3. R-41 System Balances and Results

<u>NO₃ Balance</u>		
Input:	3066 g moles	
Recovery:		
Condensate	3458 g moles	101.5%
Solid	163 g moles	4.8%
Evap.	82 g moles	2.4%
Off-gas	-	-
		<hr/> 108.7%
 <u>Fe Balance</u>		
Input:	195 g moles	
Recovery:		
Condensate	0.8 g moles	0.4%
Solid	148 g moles	77.1%
Evap.	0.2 g moles	0.1%
		<hr/> 77.6%
 <u>Na Balance</u>		
Input:	189 g moles	
Recovery:		
Condensate	1.0 g moles	0.5%
Solid	126 g moles	59.2%
Evap.	0.4 g moles	0.1%
		<hr/> 59.8%
 <u>Ca Balance</u>		
Input:	335 g moles	
Recovery:		
Condensate	-	-
Solid	421 g moles	125.6%
Evap.	0.9 g moles	0.3%
		<hr/> 125.9%
 <u>SO₄ Balance</u>		
Input:	403 g moles	
Recovery:		
Condensate	2.4 g moles	0.6%
Solid	268 g moles	66.5%
Evap.	1.2 g moles	0.3%
		<hr/> 67.4%
 <u>Ru Balance</u>		
Input:	0.442 g moles	
Recovery:		
Condensate	-	-
Solid	0.237 g moles	53.6%
Evap.	0.031 g moles	7.0%
		<hr/> 60.6%

Table 6.3. Continued

Average Feed Rate

$$391/6 = 65.17 \text{ liter/hr average}$$

Water Feed Rate

$$1453 \text{ liter of water, water to feed ratio} = 3.7$$

Calcined Solids

$$80 \text{ kg solid}/60 \text{ liters} = 1.33 \text{ g/cc bulk density}$$

Table 6.4. Test Results for Test R-41 Purex + Ca(NO₃)₂

Test Time	Feed System	System Water Feed	Water to Feed Ratio	System Condensate	Evap Press	NO ₃ Input	NO ₃ Condensate	Evap Density	Evap Temp	Evap Steam Temp	Evap Steam Cond	Evap H ⁺ Conc	Evap Fe Conc	Evap Ru Conc
hrs	liters	liters	Ratio	liters	psig	g mol	g mol	g/cc	°C	°C	liters	molar	g/l	g/l
1	135	121	0.89	229	-1.0	891	387	1.20	110.5	127	306	5.5	39.86	0.147
2	195	140	0.72	360	-1.1	1287	859	1.36	113.4	125	501	5.8	25.08	0.157
3	272	201	0.74	519	-1.0	1795	1353	1.32	113.0	150	621	7.1	57.76	0.331
4	330	288	0.87	690	-1.0	2178	1780	1.38	108.4	122	879	6.0	35.72	0.110
5	373	344	0.92	833	-1.0	2462	2160	1.31	-	110	1072	6.75	19.76	0.155
6	391	420	1.07	941	-1.0	2580	2247	1.22	107.2	113	1210	5.5	8.82	0.065
7		500	1.28	1036	-1.0		2299	1.17	104.2	112	1324	5.4	2.52	0.020
8		556	1.42	1131	-1.0		2339	1.16	104.4	111	1432	5.0	0.90	0.009
9		647	1.65	1224	-1.0		2392	1.15	104.4	113	1537	5.15	0.36	0.007
10		662	1.69	1334	-1.0		2539	1.19	107.4	115	1660	6.7	0.28	0.110
11		719	1.84	1431	-1.0		2683	1.21	107.8	113	1766	6.9	0.33	0.076
12		776	1.98	1535	-1.0		2829	1.20	107.4	112	1856	6.4	0.37	0.074
13		825	2.11	1625	-1.0		2920	1.19	107.4	111	1941	6.4	0.40	0.149
14		878	2.25	1710	-1.0		2993	1.19	106.6	111	2019	6.15	0.44	0.154
15		931	2.38	1797	-1.0		3052	1.18	106.0	113	2099	5.9	0.47	0.145
16		984	2.52	1890	-1.0		3112	1.17	105.8	110	2183	5.5	0.49	0.156
17		1037	2.65	1968	-1.0		3157	1.17	106.0	110	2253	5.2	0.52	0.150
18		1086	2.78	2058	-1.0		3199	1.16	104.6	109	2334	5.0	0.55	0.149
19		1139	2.91	2143	-1.0		3240	1.15	104.0	110	2409	4.75	0.55	0.153
20		1188	3.04	2228	-1.0		3270	1.14	105.0	108	2482	4.7	0.58	0.083
21		1241	3.17	2313	-1.0		3303	1.14	104.6	108	2554	4.3	0.59	0.146
22		1336	3.42	2398	-1.0		3337	1.14	103.2	107	2621	4.3	0.61	0.145
23		1347	3.45	2478	-1.0		3375	1.13	103.0	107	2686	4.2	0.61	0.136
24		1404	3.59	2558	-1.0		3412	1.13	103.0	106	2756	4.0	0.62	0.145
25		1453	3.72	2655	-1.0		3458	1.12	103.0	106	2832	3.6	0.62	0.138

Table 6.4. Continued

Test Time hrs	Calciner Heat Input KWH	Calciner Temp at Feed Point °C	Calciner Temp at Mid-Section Center °C	System Off-gas cu ft	Off-gas Before Water Scrub					Off-gas After Water Scrub					
					N ₂ vol %	O ₂ vol %	Ar vol %	N ₂ O + CO ₂ vol %	NO ₂ vol %	Air cu ft	N ₂ vol %	O ₂ vol %	Ar vol %	N ₂ O + CO ₂ vol %	NO ₂ vol %
1	73	115	115	-	77.9	20.8	0.9	-	-	-	77.7	20.7	0.9	0.4	-
2	119	150	125	-	77.9	20.9	0.9	-	-	-	72.7	25.4	0.9	0.5	-
3	165	125	125	-	76.3	22.0	0.9	0.6	-	-	77.4	21.8	0.9	0.3	-
4	205	125	125	-	76.5	21.7	0.9	0.7	-	-	75.8	22.9	0.9	0.6	-
5	256	120	120	-	75.3	23.2	0.9	0.7	-	-	76.3	22.5	0.9	0.3	-
6	304	120	120	-	76.7	21.7	0.9	0.9	-	-	77.2	21.5	0.9	0.3	-
7	351	125	125	-	77.0	21.2	0.9	0.7	-	-	77.3	21.4	0.9	0.3	-
8	402	125	125	-	77.6	21.4	0.9	0.4	-	-	77.5	21.4	0.9	0.2	-
9	449	125	125	-	77.9	20.8	0.9	0.4	-	-	77.5	21.4	0.9	0.4	-
10	498	135	125	-	63.8	35.1	0.7	0.6	0.1	-	62.0	36.5	0.7	0.6	-
11	520	310	130	-	65.4	33.1	0.8	0.5	0.5	-	66.5	31.9	0.8	0.6	-
12	536	365	140	-	68.2	30.3	0.8	0.6	0.5	-	66.0	32.8	0.7	0.6	-
13	551	350	150	-	68.8	29.9	0.7	0.4	0.3	-	66.1	32.8	0.7	0.4	-
14	565	350	185	-	71.0	27.7	0.8	0.3	0.2	-	71.4	27.3	0.8	0.3	-
15	581	180	260	-	78.0	21.0	0.9	-	-	-	73.5	25.6	0.9	0.4	-
16	587	145	290	-	74.7	23.9	0.9	0.6	0.1	-	75.1	23.7	0.9	0.2	-
17	598	140	375	-	-	-	-	-	-	-	-	-	-	-	-
18	608	145	545	-	75.3	23.4	0.9	0.5	-	-	76.1	22.9	0.9	0.2	-
19	616	145	610	-	75.8	22.9	0.9	0.3	-	-	75.7	23.2	0.9	0.3	-
20	625	145	670	-	76.0	22.5	0.9	0.6	-	-	76.9	22.2	0.9	0.1	-
21	635	355	725	-	74.0	24.5	0.9	0.6	0.2	-	76.2	22.7	0.9	0.1	-
22	647	450	745	-	69.1	29.0	0.8	0.6	0.4	-	77.3	22.0	0.9	-	-
23	656	480	775	-	66.5	32.0	0.8	0.4	0.1	-	61.4	37.4	0.8	0.6	-
24	666	485	805	-	62.0	35.6	0.7	1.6	0.1	-	66.0	32.7	0.8	0.5	-
25	679	505	835	-	60.5	37.0	0.7	0.6	1.1	-	78.1	21.0	0.9	-	-

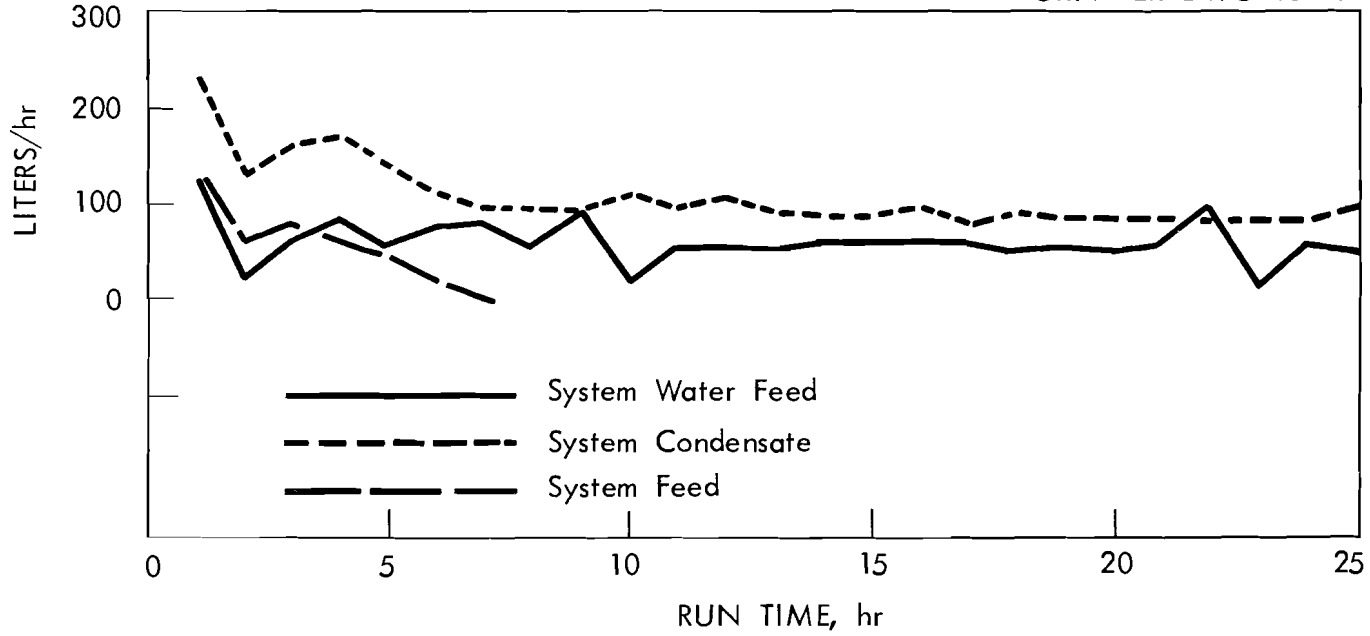


Fig. 6.1. Flow rates for Test R-41.

Of the sulfate recovered, 99% was in the solid.

The ruthenium in the evaporator condensate was below detectable limits (less than 0.001 g/liter).

6.3 Evaporator and Calciner Control

The evaporator was about in control when the evacuation drill occurred. The shutdown and start-up caused an upset which lasted for 3 to 5 hours. The calciner feed line and liquid level probe lines had solids calcined on them during the shutdown, causing malfunction throughout the test.

The control settings for the test are given in Table 6.5. The evaporator temperature was controlled on manual this test because it could not be adjusted properly on automatic control (Figure 6.2). The evaporator density varied from 1.38 g/cc to 1.16 g/cc (Figure 6.3). The set point was 1.30 g/cc. The evaporator liquid level control varied from a high of 80% to a low of 40%. The set point was 50% (Figure 6.4).

The wet test meter for measuring the off-gas volume corroded out at the start of the test, therefore the off-gas volumes are unknown.

6.4 Calcined Solids

The solids from 391 liters of feed plus 109 liters of 3 M $\text{Ca}(\text{NO}_3)_2$ weighed 80 kg. The bulk density of 1.33 was calculated on a basis of ~60 liters of volume to the liquid level control point. About 10% of the volume actually was a cone shaped hole down the center of the solid. From the solid analysis (Table 6.6), it appeared that the sulfate migrated to the bottom and the solid at the bottom was very hard. The bottom maximum temperature was 850°C, the top was 500°C. There was no evidence of internal calciner pot corrosion in this test.

Table 6.5. Control Settings for Test R-41

Evap. density	controlling	feed addition	
Evap. liquid level	controlling	steam heating	
Evap. temperature	controlling	water addition	
Evap. pressure	controlling	off-gas by-pass	
Calciner liquid level	controlling	calciner feed	
	Set Point %	Prop. Band %	
		Reset Rate min	
Evap. density	60-70	90	5
Evap. liquid level	50	200	5
Evap. temperature	33	Manual	
Evap. pressure	40	25	0.3
Calciner liquid level	50	200	5

Table 6.6. R-41 Solid Analysis

	Fe wt %	SO ₄ wt %	Ru wt %	Al wt %	Ca wt %	Na wt %	NO ₃ wt %	Mg wt %
Top	8.18	25.5	0.024	1.23	19.9	3.12	19.0	< 0.1
Center	7.00	22.6	0.034	1.24	31.0	1.35	18.9	< 0.1
Bottom	15.8	48.6	0.033	1.26	12.4	6.42	0.9	< 0.1
Average	10.33	32.2	0.030	1.24	21.1	3.63	12.9	< 0.1

UNCLASSIFIED
ORNL-LR-DWG 65318

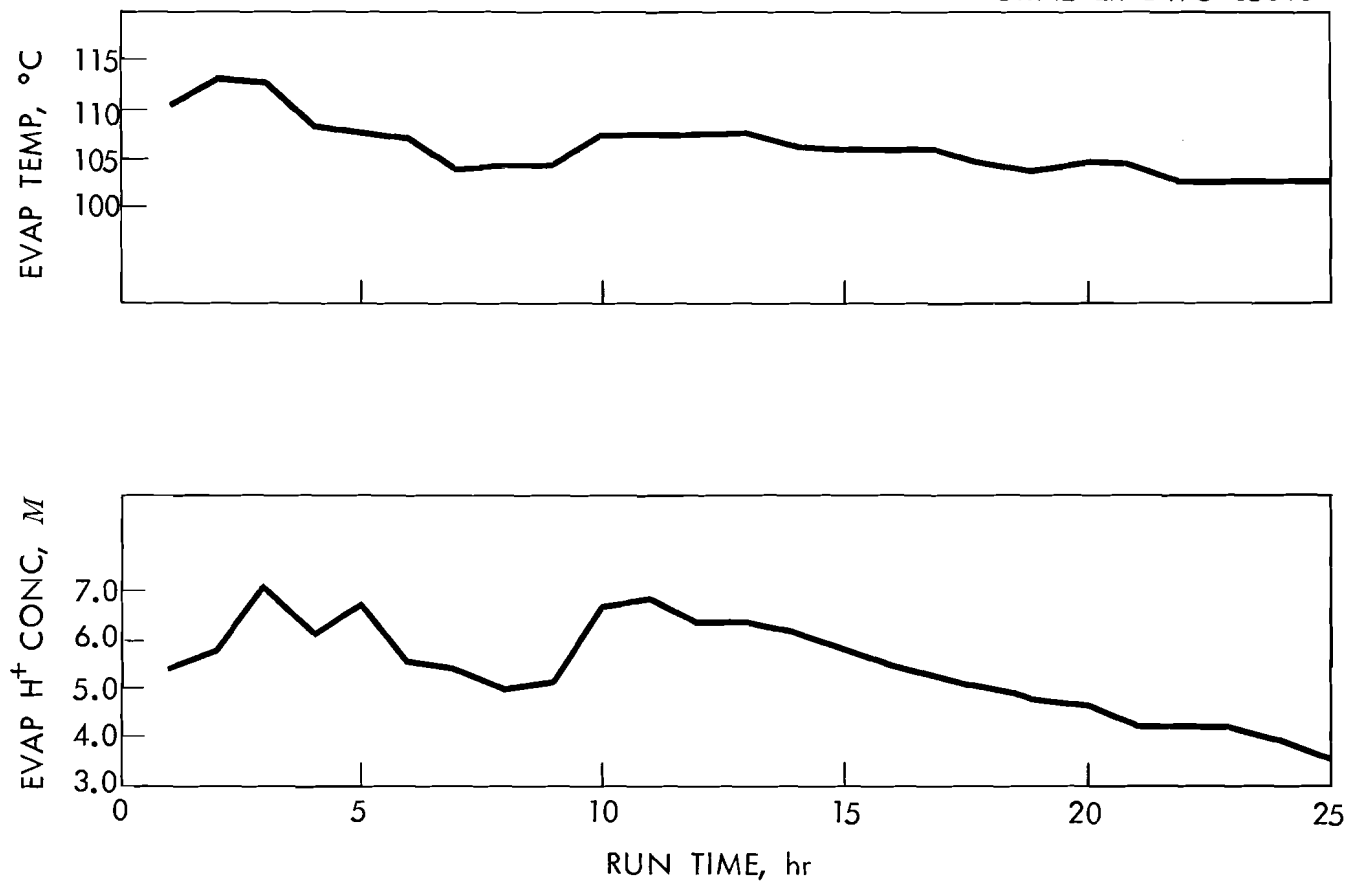


Fig. 6.2. Evaporator temperature control and acid concentration for Test R-41.

UNCLASSIFIED
ORNL-LR-DWG 65319

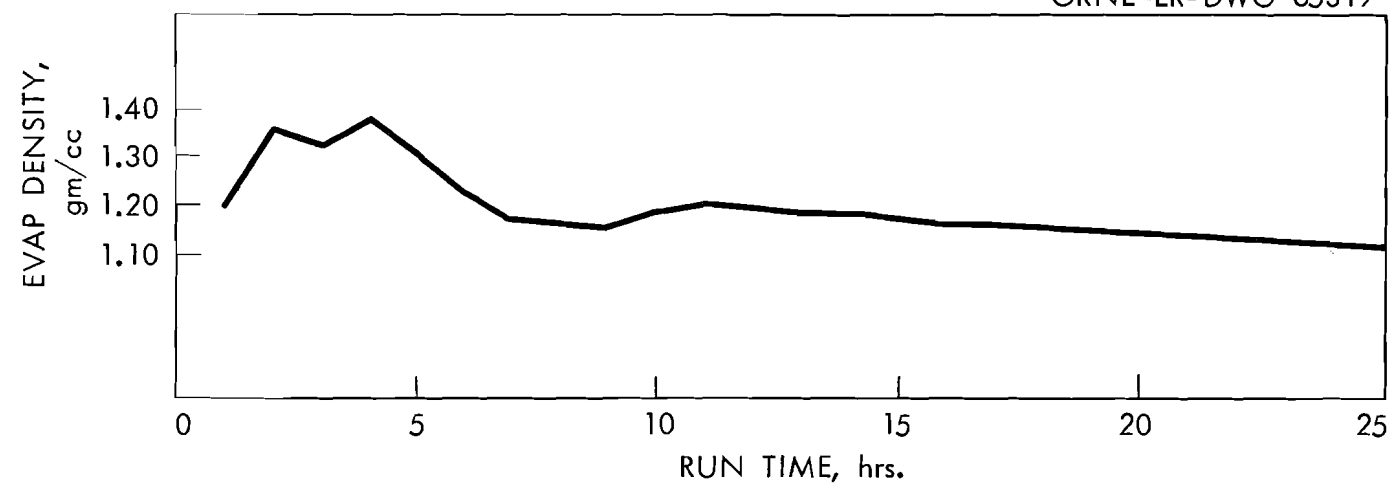


Fig. 6.3. Evaporator density control for Test R-41.

UNCLASSIFIED
ORNL-LR-DWG 65320

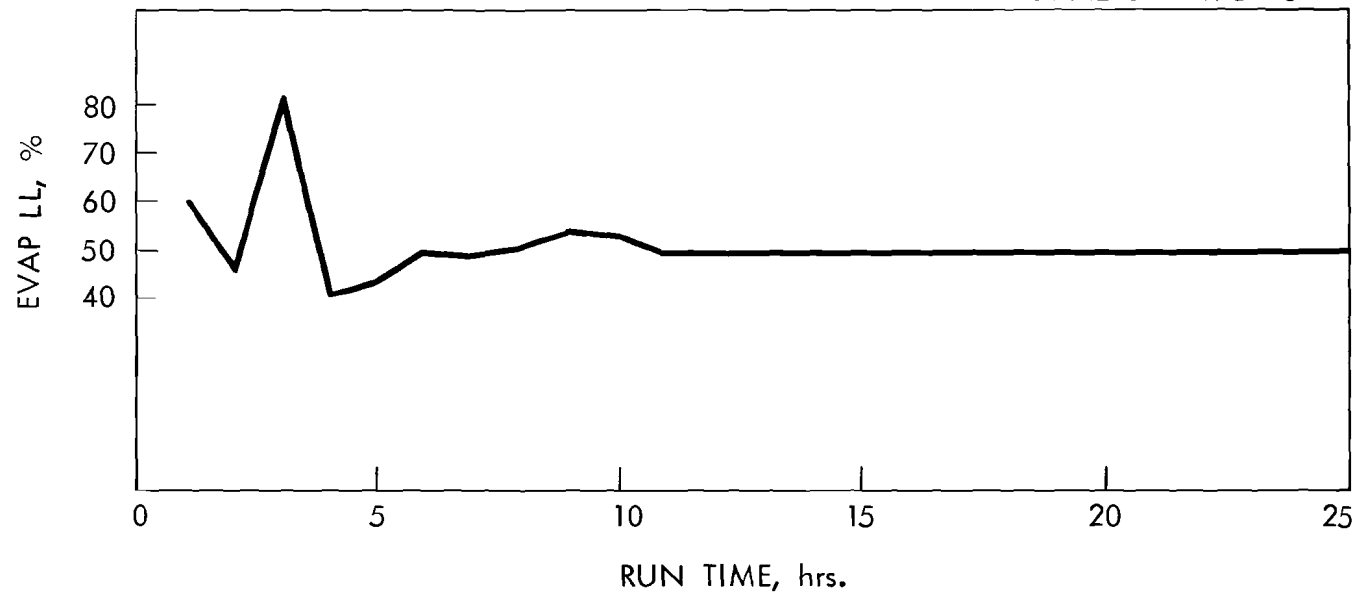
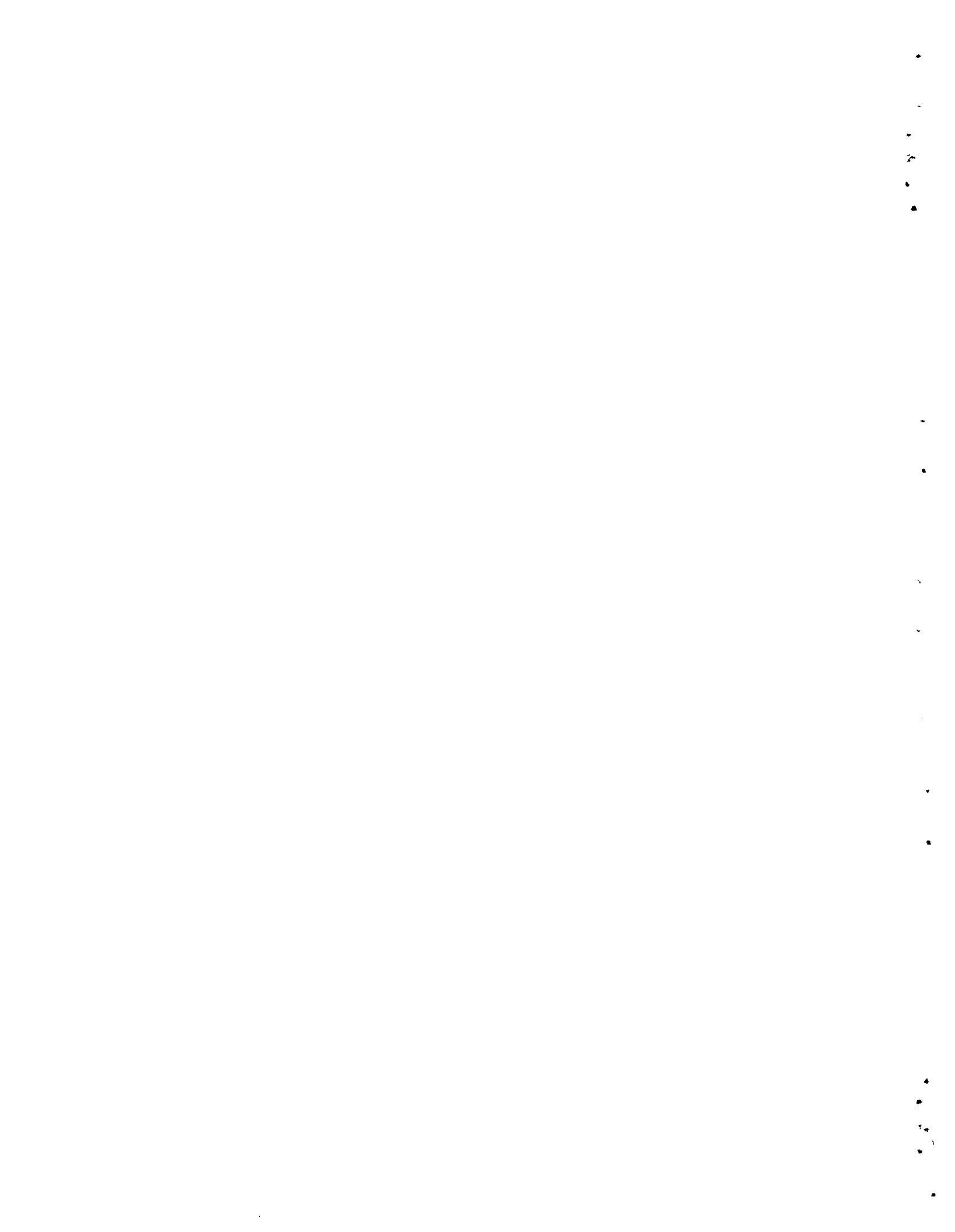


Fig. 6.4. Evaporator liquid level control for Test R-41.



DISTRIBUTION

- | | | | |
|-------|-----------------------------------|----------|---------------------------------------|
| 1. | E. L. Anderson (AEC Washington) | 54. | J. A. Lieberman (AEC Washington) |
| 2. | F. P. Baranowski (AEC Washington) | 55. | R. B. Lindauer |
| 3. | W. G. Belter (AEC Washington) | 56. | A. P. Litman |
| 4. | S. Bernstein (Paducah) | 57. | J. T. Long |
| 5. | R. E. Blanco | 58. | B. Manowitz (BNL) |
| 6. | J. O. Blomeke | 59. | J. L. Matherne |
| 7-10. | J. C. Bresee | 60. | J. A. McBride (ICPP) |
| 11. | R. E. Brooksbank | 61. | J. P. McBride |
| 12. | K. B. Brown | 62. | W. T. McDuffee |
| 13. | F. R. Bruce | 63. | R. A. McGuire (ICPP) |
| 14. | J. A. Buckham (ICPP) | 64. | R. A. McNees |
| 15. | L. P. Bupp (HAPO) | 65. | R. P. Milford |
| 16. | W. D. Burch | 66. | J. W. Morris (SRP) |
| 17. | W. H. Carr | 67. | E. L. Nicholson |
| 18. | G. I. Cathers | 68. | J. R. Parrott |
| 19. | J. T. Christy (HOO) | 69. | F. S. Patton, Jr. (Y-12) |
| 20. | W. E. Clark | 70. | H. Pearlman (AI) |
| 21. | V. R. Cooper | 71. | R. H. Rainey |
| 22. | K. E. Cowser | 72. | J. T. Roberts (IAEA, Vienna, Austria) |
| 23. | F. E. Croxton (Goodyear Atomic) | 73. | K. L. Rohde (ICPP) |
| 24. | F. L. Culler, Jr. | 74. | C. A. Rohrmann (HAPO) |
| 25. | W. Davis, Jr. | 75. | A. D. Ryon |
| 26. | O. C. Dean | 76. | W. F. Schaffer, Jr. |
| 27. | D. E. Ferguson | 77-79. | E. M. Shank |
| 28. | L. M. Ferris | 80. | M. J. Skinner |
| 29. | R. J. Flanary | 81. | C. M. Slansky (ICPP) |
| 30. | E. R. Gilliland (MIT) | 82. | S. H. Smiley (ORGDP) |
| 31. | H. E. Goeller | 83. | J. I. Stevens (ICPP) |
| 32. | M. J. Googin (Y-12) | 84. | C. E. Stevenson (ANL, Idaho) |
| 33. | H. B. Graham | 85. | K. G. Steyer (General Atomics) |
| 34. | A. T. Gresky | 86. | E. G. Struxness |
| 35. | P. A. Haas | 87. | J. C. Suddath |
| 36. | M. J. Harmon (HAPO) | 88. | J. A. Swartout |
| 37. | F. E. Harrington | 89. | F. M. Tench (Y-12) |
| 38. | L. P. Hatch (BNL) | 90. | V. R. Thayer (duPont, Wilmington) |
| 39. | O. F. Hill (HAPO) | 91. | W. E. Unger |
| 40. | J. M. Holmes | 92. | J. Vanderryn (AEC ORO) |
| 41. | R. W. Horton | 93. | F. M. Watzel (ICPP) |
| 42. | A. R. Irvine | 94. | C. D. Watson |
| 43. | G. Jasny (Y-12) | 95-124. | M. E. Whatley |
| 44. | H. F. Johnson | 125. | G. C. Williams |
| 45. | W. H. Jordan | 126. | R. H. Winget |
| 46. | S. H. Jury | 127. | C. E. Winters |
| 47. | K. K. Kennedy (IDO) | 128. | R. G. Wymer |
| 48. | B. B. Klima | 129-130. | Central Research Library |
| 49. | E. Lamb | 131-134. | Laboratory Records |
| 50. | D. M. Lang | 135. | Laboratory Records (RC) |
| 51. | S. Lawroski (ANL) | 136. | Document Reference Section |
| 52. | R. E. Leuze | 137. | Research and Development Division |
| 53. | W. H. Lewis | 138-152. | DTIE |

